Uncertainty propagation with B-spline based interval field decomposition method in boundary value problems

Han Hu, Yi Wu, Anas Batou, Huajiang Ouyang

Uncertainty propagation with B-spline based Interval Field Decomposition method in boundary value problems

Han Hu[a], Yi Wu[b,c], Anas Batou[b,*], Huajiang Ouyang[a]

[a] *Department of Mechanical, Materials and Aerospace Engineering, School of Engineering, University of Liverpool, Liverpool L69 7ZF, United Kingdom*
[b] *MSME, Univ Gustave Eiffel, CNRS UMR 8208, Univ Paris Est Creteil, F-77474 Marne-la-Vallée, France*
[c] *State Key Laboratory of Advanced Design and Manufacturing for Vehicle Body, Hunan University, Changsha, 410082, China*

Abstract

In this paper, uncertainty propagation problems are addressed by modelling the non-deterministic parameters as an interval field to account for spatial dependency. The interval field is constructed using a recently proposed B-spline based interval field decomposition method, which is related to an explicit formulation composed of B-spline basis functions and corresponding interval field coordinates, which can be incorporated directly into the governing equation of the boundary value problems. The solution to the governing equation can be approximated by a B-spline basis expansion using the collocation method taking advantage of high-degree continuity of B-spline basis functions. In this way, the crisp bounds of the output can be effectively accounted for. Numerical cases are provided to illustrate the effectiveness of the proposed method. The impact of the influence radius, the results obtained using an interval variable model and the combined impact of multiple uncertain parameters are also studied. Furthermore, for discretised problems, the interval field finite element formulation is presented and the resulting bounds of the output are determined by the Neumann expansion method, by which the extreme values can be effectively approximated.

Keywords: Interval field, uncertainty propagation, boundary value problems, interval field finite element method

1. Introduction

Uncertainties in parameters are present in nearly all practical engineering problems, posing substantial challenges to predicting realistic responses and designs. Solutions to such problems are often sought traditionally through probability theory by quantifying the uncertainties in a probabilistic approach [1, 2]. However, the determination of the Probability Density Function (PDF) demands a large amount of experimental data, which is often unavailable in reality. As a result, non-probabilistic methods emerge as viable alternatives [3, 4] that can evaluate the performance of a system under investigation without the need for a PDF. Typical methods included in the non-probabilistic approaches are interval analysis [5–7], fuzzy set

*Corresponding author
Email address: batoua@liverpool.ac.uk (Anas Batou)

Nomenclature

Abbreviations

BIFD	B-spline based interval field decomposition
IDW	Inverse Distance Weighting
IFCs	Interval field coordinates
Lb	Lower bound
LIFD	Local interval field decomposition
MC	Monte-Carlo
PDEs	Partial Differential equations
PDF	Probability Density Function
Ub	Upper bound

Symbols

$\boldsymbol{\sigma}_{\mathrm{e}}^{(n)}$	n-th order approximation of the elemental stress vector
κ^{I}	Interval field of thermal conductivity
$\mathbb{E}^{\mathrm{I}}$	Interval filed of Young's modulus
$\mathbf{B}$	The strain-displacement matrix
$\mathbf{D}^{\mathrm{I}}$	Non-deterministic elasticity matrix
$\mathbf{K}_{\mathrm{e}}^{\mathrm{I}}$	Non-deterministic element stiffness matrix
$\mathbf{T}_{\mathrm{e}}$	Local-global transformation matrix
$\mathbf{T}_{\mathrm{e}}$	Transformation matrix for local to global stiffness matrix
$\mathbf{u}_{(n)}$	n-th order approximation of the displacement vector
ν^{I}	Interval filed of kinematic viscosity
ξ_i^{I}	Interval field coordinates
Ξ	Knot vector
$B_{i,k}$	The i-th B-spline function of degree k
D_T	Measure of temperature variability
D_u	Measure of displacement variability
H_c	Interval center
H_r	Interval radius
h	Mesh size
$I(x)$	Moment of inertia of the beam cross-section
$p^{\mathrm{I}}(x, \boldsymbol{\eta})$	Interval filed of external transverse load
R_d	Influence radius

theory [8, 9] and evidence theory [10, 11], to name a few. In these methods, the PDF of the input is replaced by the upper and lower bounds of the input parameters. When inputs become multi-dimensional, the output bounds can be obtained through vertex analysis [12, 13] since the assumption is made that there is no mutual dependency among input variables. Such an assumption may lead to the *dependency phenomenon* [14], which often results in over-conservative results.

Other important issues related to the *dependency phenomenon* are the inability to take into account spatial dependencies while modelling position-related uncertainties, such as inhomogeneous material properties, and the intensive computational cost of the vertex analysis. To tackle such problems, Moens et al [15] proposed the concept of 'interval field' that models the uncertain parameters as spatially correlated interval variables distributed in the field. The original form of the interval field formulation is explicit, composed of several pre-defined control points and basis functions. This formulation uses the Inverse Distance Weighting

(IDW) interpolation method, with weightings inversely related to the distances between the local point and control points. Further extensions involve improvements in its capability to address the local effects [16, 17]. Another explicit formulation of modelling an interval field is the Local interval field decomposition (LIFD) method [18], in which a set of piecewise second-order polynomial functions is set as the basis functions. The LIFD method accounts for the local effects at the cost of an increased computational burden. Recently, the authors of the present paper proposed the B-spline based interval field decomposition (BIFD) method [19], in which the basis functions are chosen as continuity-manipulatable B-spline basis functions. Apart from a more intuitive expression that directly shows the interval properties of the field, the fast evaluation of B-spline functions facilitates the modelling of complicated multi-dimensional problems. This paper investigates extensions of the BIFD method and demonstrates that this formulation of the interval field can be readily incorporated into the governing equation of the system under investigation, facilitating the analysis of uncertainty propagation by providing closed-form solutions for output bounds in some cases.

It should be noted that other interval field modeling formulations, besides explicit ones, are available in the literature, for instance, the K-L expansion based formulation [20, 21] and the convex descriptors based formulation [22, 23]. These methods typically require the eigenpair of the knowledge-based correlation functions, often adopting a set of truncated terms to reduce the dimension of the problem at the cost of restricting the source of uncertainties to a few interval coordinates. For an extensive overview of interval field formulations, readers can refer to [24].

A key research topic in interval field modelling is the uncertainty propagation through a system, which is often termed the forward problem. Many investigations on forward problems have been conducted with uncertain parameters modelled using various interval field formulations introduced above. Sofi [25] studied the Euler-Bernoulli beams subjected to static loads with interval-field-modelled elastic properties predicting the bounds of the transversal displacement. Jiang et al [26] investigated the dynamic responses of a vibration system with multiple degrees of freedom subjected to time-varying external loads, modelled as an interval process. Chen et al [27] studied the dynamic response of a simplified dynamic finite element model of a lunar lander with its Young's modulus modelled as a 1D interval field. Although these studies demonstrate that interval field formulations can be effectively integrated into systems and account for crisp output bounds, few can directly work with Partial Differential equations (PDEs) in boundary value problems, typically requiring a discretised system equation. This paper demonstrates that, by using the BIFD method, the system equation can integrate the interval field formulation, and can be solved using the collocation method, with the approximated solution represented by a B-spline basis expansion, which is computationally manageable thanks to the high continuity of B-spline basis functions. Moreover, in specific scenarios, the output bounds can be predicted using optimisation methods or approximation methods without requiring Monte-Carlo (MC) simulations. In addition to those approaches, a new interval field finite element method has been proposed for addressing uncertainty propagation in practical engineering problems.

The remainder of this paper is organised as follows. Section 2 briefly reviews the BIFD formulation.

Section 3 investigates a sequence of boundary value problems. First, a steady-state heat conduction problem is studied to illustrate the possibility of using an optimisation method to determine the output bounds. Next, the Burgers' equation with spatially varying kinematics viscosity is solved to investigate the uncertainty propagation through time and space. Lastly, an Euler-Bernoulli beam with both spatially varying Young's modulus and external loads is studied. The interval field finite element method is presented in Sec.4 with a 2D square plane case to illustrate the effective and efficient approximation of output bounds using the Neumann expansion method.

2. B-spline based interval field decomposition (BIFD) method

2.1. Interval analysis

This section provides a preliminary overview of interval analysis. An interval scalar, denoted as X^{I}, is a convex subset of the domain $\mathbb{R}$ constrained by its lower bound $\underline{X}$ and upper bound $\bar{X}$ expressed as

$$X^{\mathrm{I}} = [\underline{X}, \bar{X}] = \{X \in \mathbb{R}, \underline{X} \leq X \leq \bar{X}\}, \tag{1}$$

for which the interval centre, X_c, and the interval radius, X_r, are defined as

$$X_c = \frac{\underline{X} + \bar{X}}{2}, \; X_r = \frac{\underline{X} - \bar{X}}{2}. \tag{2}$$

An interval vector $\mathbf{X}^{\mathrm{I}} \in \mathbb{R}^{\mathrm{n}}$ is defined as a set of interval scalars as

$$\mathbf{X}^{\mathrm{I}} = \left\{ \begin{array}{c} X_1^{\mathrm{I}} \\ X_2^{\mathrm{I}} \\ \vdots \\ X_n^{\mathrm{I}} \end{array} \right\}. \tag{3}$$

The sample space of the interval vector $\mathbf{X}^{\mathrm{I}}$ is a multi-dimensional hypercube, within which each interval scalar are mutually independent. For a deterministic function $\mathbf{Y} = f(\mathbf{X})$, subjected to a vector input $\mathbf{X}$ taken values from an interval vector $\mathbf{X}^{\mathrm{I}}$, the set of all outputs can also be treated as an interval vector such as

$$\mathbf{Y}^{\mathrm{I}} = \{\mathbf{Y} \in \mathbb{R}^{\mathrm{m}} \; | Y_i \in [\underline{Y}_i, \bar{Y}_i]\}, \tag{4}$$

where

$$\underline{Y}_i = \min_{\mathbf{X} \in \mathbf{X}^{\mathrm{I}}} f_i(\mathbf{X}),$$

$$\bar{Y}_i = \max_{\mathbf{X} \in \mathbf{X}^{\mathrm{I}}} f_i(\mathbf{X}),$$

where $f_i(\mathbf{X})$ denotes the i-th output generated by $f(\mathbf{X})$. The determination of the bounds of the output interval vector usually requires global optimisation methods. The results can be conservative if the correlations within the components of the input are omitted, which leads to the so-called *dependency phenomenon*. In this regard, modelling the input as an interval field offers a feasible way to alleviate this phenomenon.

2.2. The BIFD formulation

In the 1D BIFD formulation, an interval field $\mathbb{H}^{\mathrm{I}}$ is defined as the following expansion [19]

$$\mathbb{H}^{\mathrm{I}}(x) = H_c + H_r \sum_{i=1}^{N} B_{i,k}(x)\, \xi_i^{\mathrm{I}}, x \in \Omega_D \tag{5}$$

where H_c and H_r are respectively the interval centre and interval radius, Ω_D is the continous 1D domain of interest and $\{B_{i,k}\}$ are the B-spline basis functions of degree k, which can be obtained recursively through the Cox-de Boor formula [28], such as for $k = 0$

$$B_{i,0}(x) = \begin{cases} 1 & t_i \leq x < t_{i+1} \\ 0 & \text{otherwise} \end{cases} . \tag{6}$$

and for $k > 0$

$$B_{i,k}(x) = \frac{x - t_i}{t_{i+k} - t_i} B_{i,k-1}(x) + \frac{t_{i+k+1} - x}{t_{i+k+1} - t_{i+1}} B_{i+1,k-1}(x), \tag{7}$$

where t_i is knot values taken from an equispaced knot vector $\Xi = \{t_1, t_2, ..., t_{N+k+1}\}$ that encloses the domain of interest and $\xi_i^{\mathrm{I}} = \{\xi_i | -1 \leq \xi_i \leq 1\}$ $i = 1, \ldots, N$ are unitary interval scalars that are called *interval field coordinates* (IFCs) in this paper. The space between adjacent knots $\Delta t = |t_i - t_{i+1}|$, $1 \leq i \leq N + k$ is related to the influence radius of the interval field $R_d = (k + 1)\Delta t/2$, which indicates the distance over which the B-spline basis function has a non-zero support. The value of N is determined as $N = \mathrm{ceil}(L/\Delta t)$, where L is the length of Ω_D. The B-spline basis functions have beneficial properties such as controllable continuity, linear independence, non-negativity and partition of unity. The partition of unity is vital to form a bounded field. The presented BIFD formulation can effectively model an interval field with bounds $[H_c - H_r, H_c + H_r]$ and influence radius R_d, which indicates the spatial dependency among field points. Two examples of the interval fields generated using (5) are provided in Fig.1. The algorithmic procedure to construct a 1D homogeneous interval field can be seen in Algorithm 1. For multi-dimensional interval field construction and the inhomogeneous variants, as well as the relationship between 'influence radius' and commonly used 'correlation length' in the probabilistic community, interested readers are referred to [19].

3. Uncertainty propagation in solving boundary value problems

In this section, three distinct types of boundary value problems are studied to demonstrate the implementation of the BIFD formulation directly in the boundary value problems. The approach can be applied to other types of boundary value problems.

3.1. Steady-state heat conduction problem

In this section, a 1D steady-state heat conduction problem with non-deterministic parameters is investigated. Heat conduction equations are often used for determining the spatial temperature distribution of a homogeneous material where the thermal conductivity is seen as a constant parameter [29, 30]. In the

Algorithm 1: 1D homogeneous interval field construction by BIFD

Input : Interval centre H_c, interval radius H_r, degree k.

(1) Determine the influence radius R_d and derive the knot span $\Delta t = 2R_d/(k+1)$.

(2) Extend $k\Delta t$ to the left side of the domain Ω, $|\Omega| = L$, and extend $(N+k)\Delta t - L$ to the right side of the domain, where $N = \text{ceil}(L/\Delta t)$.

(3) Discretise the extended field domain into $N + 2k$ elements with element size Δt and take all nodes to form the knot vector $\hat{\Xi}$.

(4) Build a set of B-spline basis functions of degree k with a total number N based on the knot vector Ξ.

(5) Generate realisations of $\{\xi_i\}_{i=1}^{N}$.

(6) Generate the interval field through (5).

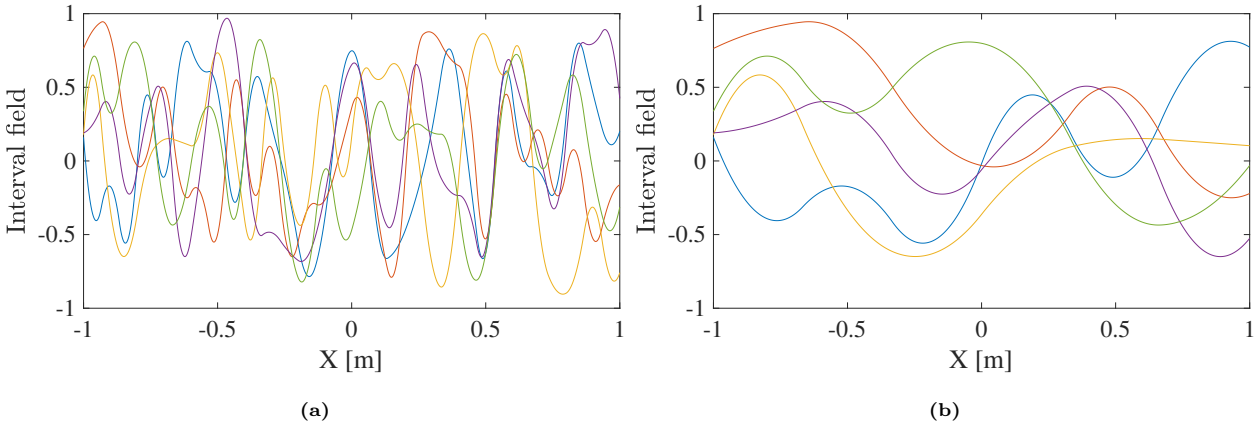

Fig. 1. Interval fields on the domain $\Omega = [-1, 1]$ with $H_c = 0$, $H_r = 1$ and (a) $R_d = 0.1$ [m]; (b) $R_d = 0.5$ [m]. Each case contains five realisations.

present case, the thermal conductivity is considered non-deterministic and is modelled as an interval field. Define the domain of interest as $\Omega = [0, L]$. The non-deterministic problem within domain Ω can be stated mathematically as

$$\begin{cases} \frac{\partial}{\partial x}[\kappa^{\mathrm{I}}(x, \boldsymbol{\xi})\, A\, \frac{\partial T}{\partial x}] + s(x) = 0 \\ T(0) = c_1,\ T(L) = c_2, \end{cases} \tag{8}$$

where A is a constant denoting the section area, c_1 and c_2 are the boundary temperature values of the system, $s(x)$ is the source term and $\kappa^{\mathrm{I}}(x, \boldsymbol{\xi})$ is the thermal conductivity, which is modelled as an interval field as

$$\kappa^{\mathrm{I}}(x, \boldsymbol{\xi}) = \kappa_c + \kappa_r \sum_{i=1}^{M} B_i(x)\, \xi_i^{\mathrm{I}}, \tag{9}$$

where κ_c and κ_r are respectively the interval centre and interval radius, $\{B_i\}_{i=1}^{M}$ is a set of cubic B-spline basis functions with an influence radius R_d, which satisfies the partition of unity on Ω and $\boldsymbol{\xi} = \{\xi_i^{\mathrm{I}}\}$ is a set of IFCs. The solutions of (8) can be represented using cubic B-spline basis functions. Let the domain Ω be divided by

a mesh size h into N elements and define a new knot vector $\hat{\Xi} = [-3h, -2h, \ldots, Nh, \ldots, (N+2)h, (N+3)h]$. A new set of cubic B-spline basis functions $\{\hat{B}_j\}_{j=1}^{N+3}$ can be defined on the basis of $\hat{\Xi}$. Note that for the accuracy purpose, $h \leq R_d/2$ should be satisfied so that $M \leq N+3$ and the local effects modelled by $\{B_i\}$ can be fully captured by $\{\hat{B}_j\}$ [19]. The approximate solution of (8) can thus be expressed as

$$T(x) = \sum_{j=1}^{N+3} \hat{B}_j(x)\, t_j, \tag{10}$$

where $\{t_j\}_{j=1}^{N+3}$ are the coefficients to be computed. Substituting (9) and(10) into $(8)_1$ and assuming the source term to be zero, the following equation is obtained as

$$(\kappa_r \sum_{i=1}^{M} B_i'(x)\, \xi_i^{\mathrm{I}})(\sum_{j=1}^{N+3} \hat{B}_j'(x)\, t_j) + (\kappa_c + \kappa_r \sum_{i=1}^{M} B_i(x)\, \xi_i^{\mathrm{I}})(\sum_{j=1}^{N+3} \hat{B}_j''(x)\, t_j) = 0. \tag{11}$$

Equation (11) can be solved using the collocation method, taking advantage of the high-degree continuity of the B-spline basis functions. Considering in total $N+3$ unknowns to be solved, $N+1$ collocation points are required together with two boundary conditions to have sufficient number of equations to calculate the unknowns. Let $\{x_k\}_{k=1}^{N+1} = \{0, h, 2h, \ldots, Nh\}$ be the set of collocation points. Let $n_c = N+3$, the whole equation set can then be written as

$$\begin{bmatrix} A_{11} & \cdots & A_{1j} & \cdots & A_{1n_c} \\ \vdots & \ddots & \vdots & \cdots & \vdots \\ A_{k1} & \cdots & A_{kj} & \cdots & A_{kn_c} \\ \vdots & \cdots & \vdots & \ddots & \vdots \\ A_{n_c1} & \cdots & A_{n_cj} & \cdots & A_{n_cn_c} \end{bmatrix} \begin{Bmatrix} t1 \\ \vdots \\ t_k \\ \vdots \\ t_{n_c} \end{Bmatrix} = \begin{Bmatrix} b_1 \\ \vdots \\ b_k \\ \vdots \\ b_{n_c} \end{Bmatrix}, \tag{12}$$

where

$$\begin{gathered} A_{kj} = (\kappa_r \sum_{i=1}^{M} B_i'(x_k)\, \xi_i)\hat{B}_j'(x_k) + (\kappa_c + \kappa_r \sum_{i=1}^{n_c} B_i(x_k)\xi_i)\hat{B}_j''(x_k),\ 1 \leq k \leq n_c - 2,\ 1 \leq j \leq n_c \\ A_{n_c-1j} = \hat{B}_j(0),\ A_{n_cj} = \hat{B}_j(L),\ 1 \leq j \leq n_c \\ b_k = 0,\ 1 \leq k \leq n_c - 2,\ b_{n_c-1} = c_1,\ b_{n_c} = c_2. \end{gathered} \tag{13}$$

The above equations can be written into matrix form as

$$\mathbf{A}\mathbf{t} = \mathbf{b}, \tag{14}$$

where

$$\mathbf{A} = \{A_{kj}\},\ \mathbf{t} = [t_1, t_2, \ldots, t_{n_c}]^{\mathrm{T}},\ \mathbf{b} = [b_1, b_2, \ldots, b_{n_c}]^{\mathrm{T}}. \tag{15}$$

Finally, the upper and lower bounds of the approximate solution $T(x)$ can be determined through an optimisation method, such as

$$\begin{gathered} \text{obj. min } \hat{\mathbf{B}}(x)^{\mathrm{T}}\mathbf{t}\ \&\max\ \hat{\mathbf{B}}(x)^{\mathrm{T}}\mathbf{t},\ \forall x \in \Omega \\ \text{s.t. } \xi_i \in [-1, 1], \end{gathered} \tag{16}$$

where $\hat{\mathbf{B}}(x) = [\hat{B}_1(x), \hat{B}_2(x), \ldots, \hat{B}_{n_c}(x)]^{\mathrm{T}}$. The authors would like to note that an explicit solution to (14) can only be achieved with acceptable time cost when the problem is in a small scale, e.g. less than 10 IFCs involved. Otherwise, the computational burden can be massive and numerical approaches would be a better choice.

To demonstrate the method, an example is analysed with parameters given as follows: $L = 2$, $R_d = 2$, $c_1 = 0$, $c_2 = 1$, $h = 1$, $\kappa_c = 1$, and $\kappa_r = 0.5$. The explicit results of $\mathbf{t}$ with respect to $\{\xi_i\}$ can be found in Appendix A. The resulting bounds are obtained and plotted in Fig.2. Note that when $\kappa_r = 0$, the problem degenerates to a deterministic one and there would be no difference between the upper bound (indicated as 'Ub-Opt' in the figure) and the lower bound (indicated as 'Lb-Opt' in the figure), since the only uncertain source is eliminated from the system. For comparison, the MC method is also used to compute the upper and lower bounds of the approximated solution with 10^6 realisations, labeled as 'Ub-MC' and 'Lb-MC' in the figure. It is observed that the bounds obtained from MC method agrees well with those obtained using the optimisation method.

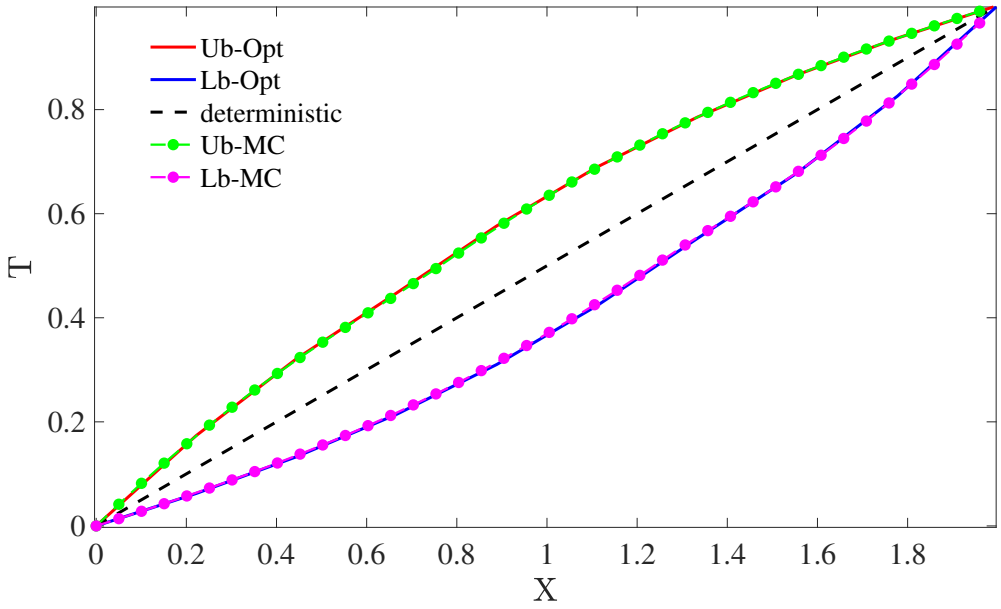

Fig. 2. Steady-state heat conduction problem, bounds obtained by optimisation method.

Note that if the thermal conductivity is modelled as an interval variable instead of an interval field, e.g. the uncertainty is not spatially dependent, the resulting temperature distribution would be no different from the deterministic case under the same conditions stated in the above example. Indeed, it can clearly be seen in (8) that when there is no source term, a spatially constant value of the thermal conductivity would be factorised and thus be eliminated from the equation. However, when taking into account the spatial variability, a clear distinction between the non-deterministic and deterministic model can be observed from the results. To quantify such a difference, a spatially averaged measure of the temperature variability can

be defined as

$$D_T = \frac{1}{L}\int_0^L \sqrt{(\mathrm{Ub}_T(x) - T_d(x))^2 + (\mathrm{Lb}_T(x) - T_d(x))^2}\,\mathrm{d}x, \tag{17}$$

where $\mathrm{Ub}_T(x)$ and $\mathrm{Lb}_T(x)$ denote respectively the upper and lower bounds of the temperature at position x and they will be mainly obtained by MC approach. $T_d(x)$ denotes the deterministic solution. The results are collected in Fig.3, which shows the development of D_T with respect to the non-dimensionalised variable R_d/L. It is foreseeable that D_T converges to zero when R_d/L is very large, as in this case the interval field degenerates to an interval variable and thus both Ub_T and Lb_T degenerate to the deterministic result. It can also be seen that D_T reaches its maximum value at around $R_d/L = 0.5$, where Ub_T and Lb_T exhibit significant differences from the deterministic results. The temperature variability is reduced as R_d/L decreases until R_d/L becomes smaller than 0.05 where D_T starts to increase afterwards. The reason for this is that when the interval field has small influence radius, the interval variables in the field only correlate to a limited range of other variables but can be quite different from variables outside the influence radius, so that in a global viewpoint the results are homogenised. However, not only the value of the interval variables but also their derivatives appear in the system equation. When the influence radius continues to decrease, the derivatives of the interval field take effect so that the homogenisation effect is deteriorated.

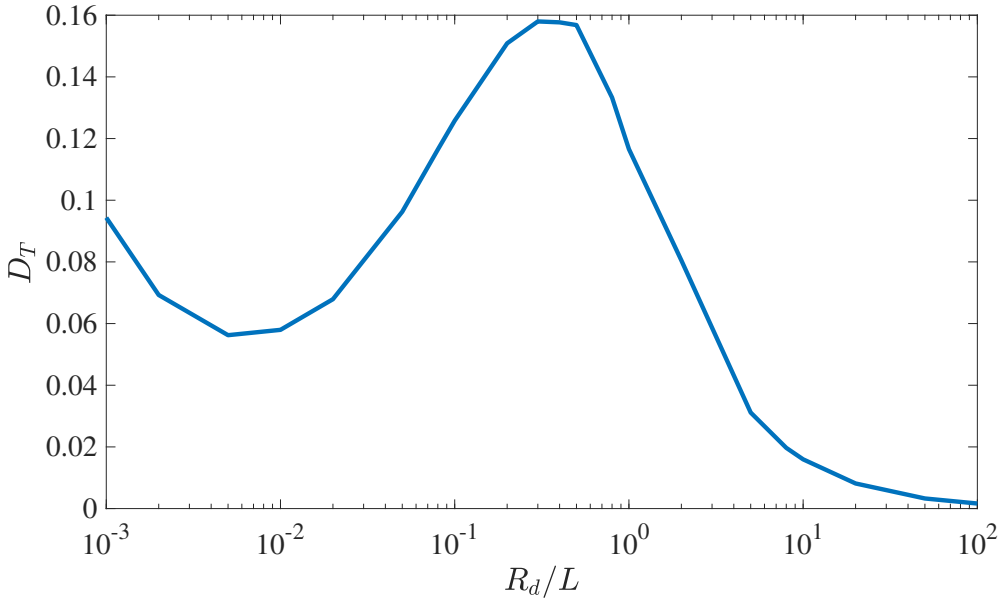

Fig. 3. Difference metric to the deterministic results of the steady-state heat conduction problem.

3.2. The Burgers' equation problem

In this section, the Burgers' equation with spatially varying kinematic viscosity is under investigation. The Burgers' equation arises in various physical problems such as viscous flow and turbulence, shock wave propagation and gas dynamics. For decades, plenty of efforts have been made to efficiently solve the Burgers' equation and various numerical approaches have been proposed [31–33]. Particular attention is paid in this

work to model the kinematic viscosity as an interval field and to study uncertainty propagation in both time and space. To achieve this goal, the BIFD method is used to model the interval field and the collocation method with cubic B-spline basis functions is used for solving the nonlinear boundary value problem.

The non-deterministic Burgers' equation on domain $\Omega = [0, L]$ is expressed as

$$\frac{\partial u}{\partial t} + \alpha u \frac{\partial u}{\partial x} = \nu^{\mathrm{I}}(x, \boldsymbol{\xi}) \frac{\partial^2 u}{\partial x^2}, \ x \in \Omega, \ t \in [0, T], \tag{18}$$

with the initial and boundary conditions as

$$\begin{cases} u(x, 0) = h_0(x), \ x \in \Omega \\ u(0, t) = g_0(t), \ u(L, t) = g_L(t), \ t \in [0, T], \end{cases} \tag{19}$$

where α is a positive constant and $\nu^{\mathrm{I}}(x, \boldsymbol{\xi})$ is the kinematic viscosity and is considered to vary spatially with bounds as

$$\nu^{\mathrm{I}}(x, \boldsymbol{\xi}) = \nu_c + \nu_r \sum_{i=1}^{M} B_i(x) \, \xi_i^{\mathrm{I}}, \tag{20}$$

where ν_c and ν_r are the interval centre and interval radius, respectively, $\{B_i\}_{i=1}^{M}$ are a set of cubic B-spline basis functions satisfying partition of unity on Ω with an influence radius R_d, and $\boldsymbol{\xi} = \{\xi_i^{\mathrm{I}}\}$ are a set of IFCs. To solve equations (18), as performed in the last case, the domain Ω is discretised into N elements with mesh size h ($h \leq R_d/2$) to form a knot vector $\hat{\Xi} = [-3h, -2h, \ldots, Nh, \ldots, (N+2)h, (N+3)h]$. A set of cubic B-spline basis functions $\{\hat{B}_j\}_{j=1}^{N+3}$ can be defined based on $\hat{\Xi}$ and it forms a basis on Ω. To form a diagonally dominant coefficient matrix of the system for handling Dirichlet boundary conditions [31], the following modifications are performed to get a new set of basis functions $\{\tilde{B}_j\}_{j=1}^{N+1}$ as

$$\begin{cases} \tilde{B}_1(x) = 2\hat{B}_1(x) + \hat{B}_2(x) & \text{for } j = 1 \\ \tilde{B}_2(x) = \hat{B}_3(x) - \hat{B}_1(x) & \text{for } j = 2 \\ \tilde{B}_j(x) = \hat{B}_{j+1}(x) & \text{for } j = 3, \ldots, N-1 \\ \tilde{B}_N(x) = \hat{B}_{N+1}(x) - \hat{B}_{N+3}(x) & \text{for } j = N \\ \tilde{B}_{N+1}(x) = \hat{B}_{N+2}(x) + 2\hat{B}_{N+3}(x) & \text{for } j = N+1. \end{cases} \tag{21}$$

The approximation to the exact solution of (18) can thus be represented as

$$\tilde{u}(x, t) = \sum_{j=1}^{N+1} \tilde{B}_j(x) \, u_j(t), \ x \in \Omega, \ t \in [0, T]. \tag{22}$$

Let the knots within Ω, e.g. $\{x_j\} = \{0, h, \ldots, (N-1)h, Nh\}$, be the collocation points. The approximate time derivative of the ith collocation point at time t is represented by $(\tilde{u}_t)_i$. Using (22) and the modified basis functions (21), the time derivatives at the collocation points are obtained as

$$\begin{cases} (\tilde{u}_t)_1 = \dot{g}_0(t) & \text{for } j = 1 \\ (\tilde{u}_t)_j = \sum_{l=1}^{N+1} \dot{u}_l \, \tilde{B}_l(x_j) & \text{for } j = 2, \ldots, N \cdot \\ (\tilde{u}_t)_{N+1} = \dot{g}_L(t) & \text{for } j = N+1 \end{cases} \tag{23}$$

Taking into account (18) and (20), (23) becomes

$$\begin{cases} \sum_{l=1}^{N+1} \dot{u}_l \, \tilde{B}_l(0) = & \dot{g}_0(t) \;\; \text{for } j = 1 \\ \sum_{l=1}^{N+1} \dot{u}_l \, \tilde{B}_l(x_j) = & -\alpha(\sum_{j=1}^{N+1} \tilde{B}_j(x) \, u_j(t))(\sum_{j=1}^{N+1} \tilde{B}'_j(x) \, u_j(t)) + (\nu_c + \nu_r \sum_{i=1}^{M} B_i(x_j) \, \xi_i^{\mathrm{I}})(\sum_{j=1}^{N+1} \tilde{B}''_j(x) \, u_j(t)) \\ & \text{for } j = 2, \ldots, N \\ \sum_{l=1}^{N+1} \dot{u}_l \, \tilde{B}_l(L) = & \dot{g}_L(t) \;\; \text{for } j = N+1 \end{cases}. \tag{24}$$

Note that for cubic B-spline basis functions, their evaluations together with the first and second derivatives at the collocation points are summarised in Table.1. The coefficient matrix for the system of ordinary

Table 1: Evaluations and derivatives of B-spline basis functions at knots $x_j, \; 2 \leq j \leq N$.

x	x_{j-2}	x_{j-1}	x_j	x_{j+1}	x_{j+2}
$\tilde{B}_j(x)$	0	$1/6$	$2/3$	$1/6$	0
$\tilde{B}'_j(x)$	0	$1/2h$	0	$-1/2h$	0
$\tilde{B}''_j(x)$	0	$1/h^2$	$-2/h^2$	$1/h^2$	0

differential equations can be obtained as

$$\mathbf{C}\dot{\mathbf{u}} = \mathbf{d}, \tag{25}$$

where

$$\mathbf{C} = \begin{bmatrix} 1 & 0 & & & \\ 1/6 & 2/3 & 1/6 & & \\ & \cdots & \cdots & \cdots & \\ & & \cdots & \cdots & \cdots \\ & & 1/6 & 2/3 & 1/6 \\ & & & 0 & 1 \end{bmatrix}, \dot{\mathbf{u}} = \begin{bmatrix} \dot{u}_1 \\ \dot{u}_2 \\ \cdots \\ \cdots \\ \dot{u}_N \\ \dot{u}_{N+1} \end{bmatrix}, \mathbf{d} = \begin{bmatrix} d_1 \\ d_2 \\ \cdots \\ \cdots \\ d_N \\ d_{N+1} \end{bmatrix},$$

$d_1 = \dot{g}_0(t), \quad \text{for } j = 1$

$$d_j = -\alpha/6(u_{j-1}(t) + 2u_j(t) + u_{j+1}(t))1/2h(u_{j-1} - u_{j+1}) + (\nu_c + \nu_r \sum_{i=1}^{M} B_i(x_j) \, \xi_i^{\mathrm{I}})1/h^2(u_{j-1} - 2u_j + u_{j+1})$$

$\text{for } j = 2, \ldots, N$

$d_{N+1} = \dot{g}_L(t), \quad \text{for } j = N+1.$

The complete solution of (18) can be determined by solving (25) with an initial displacement vector $\mathbf{u}_0$ being determined by the initial and boundary conditions (19) as

$$\mathbf{C}\mathbf{u}^0 = \mathbf{b}^{\mathbf{0}} \tag{26}$$

where

$$\mathbf{u}^0 = \begin{bmatrix} u_1^0 \\ u_2^0 \\ \cdots \\ u_N^0 \\ u_{N+1}^0 \end{bmatrix}, \mathbf{d}^0 = \begin{bmatrix} g_0(0) \\ h_0(x_2) \\ \cdots \\ h_0(x_N) \\ g_L(0) \end{bmatrix}.$$

By sampling the IFCs $\{\xi_i^{\mathrm{I}}\}$ through the MC approach for the realisations of the kinematic viscosity interval field, the uncertainty propagation is investigated in the process of solving the system equations. During the process, the upper bound $\mathrm{Ub}_u(x,t)$ and lower bound $\mathrm{Lb}_u(x,t)$ of the solution are obtained and compared with the deterministic result $u_d(x,t)$, in which the interval radius ν_r is set to zero. Like (17), a deviation metric D_u is defined to quantify the propagation of uncertainty with time as

$$D_u(t) = \frac{1}{L}\int_0^L \sqrt{(\mathrm{Ub}_u(x,t) - u_d(x,t))^2 + (\mathrm{Lb}_u(x,t) - u_d(x,t))^2}\,\mathrm{d}x, \tag{27}$$

An example is presented here to illustrate the use of the method mentioned above. The parameters used in the example are set as follows: $L = 2$, $T = 1$, $\alpha = 2$, $\nu_c = 0.6$, $\nu_r = 0.2$ and $R_d = 1$. The initial and boundary conditions are given as

$$h_0(x) = \frac{2\nu\pi \sin \pi x}{\alpha + \cos \pi x}\ (\alpha > 1) \text{ and } g_0(t) = 0,\ g_L(t) = 0. \tag{28}$$

The analytical solution to the deterministic problem ($\nu_r = 0$) is

$$u(x,t) = \frac{2\nu_c \pi \mathrm{e}^{-\pi^2 \nu_c t} \sin \pi x}{\alpha + \mathrm{e}^{-\pi^2 \nu_c t} \cos \pi x}. \tag{29}$$

In this case, a total number of 10^5 realisations are performed by the MC approach, and at each time step the upper and lower bounds of the results (indicated by 'Ub-IF' and 'Lb-IF') are determined and compared with the upper and lower bounds obtained by modelling ν as an interval variable (indicated by 'Ub-IV' and 'Lb-IV') and the deterministic result, as shown in Fig.4. It can be observed that in general the bound curves of the interval variable case are enclosed by those of the interval field case, yielding conservative results. Besides, at the initial time step, there are three positions in which the values are deterministic: two boundaries and the middle position ($x = 1$), where Ub-IF (Ub-IV) and Lb-IF (Lb-IV) are equal to the deterministic result due to the enforcement of the initial condition. As time progresses, the results of the interval variable model and the deterministic model are fixed at the middle position, whereas those of the interval field model are not. Consequently, the most significant differences between the results from the interval field and the interval variable model are the bounds in the proximity of the middle position, where the bounds of the results of the interval variable model are apparently narrower than those of the interval field model.

A further analysis is conducted regarding the propagation of the difference metric D_u with time for various influence radii, as depicted in Fig.5. It shows that the influence radii of the kinematic viscosity

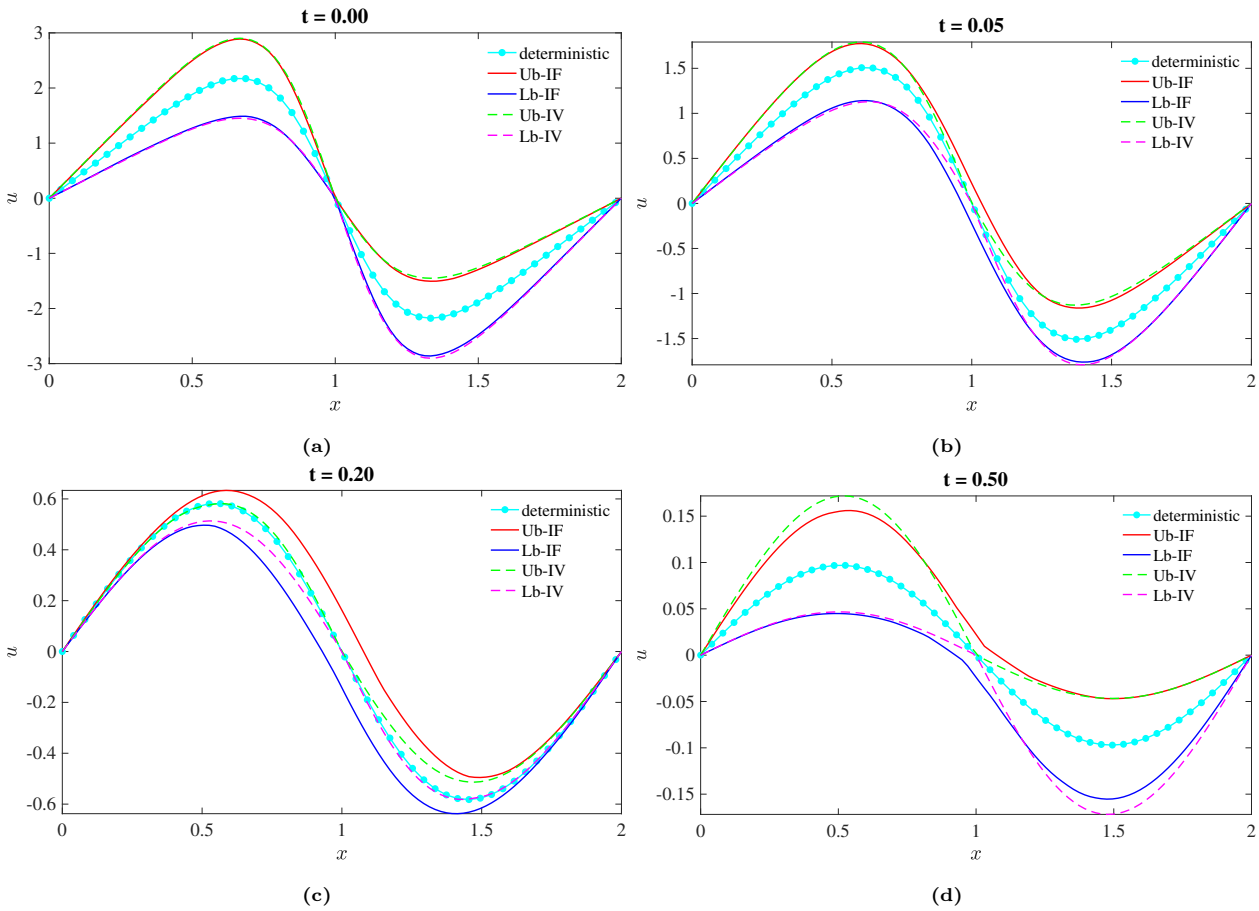

Fig. 4. Time snapshot of the solutions to the Burgers' equation in the example at (a) $t = 0.00$; (b) $t = 0.05$; (c) $t = 0.20$; (d) $t = 0.50$.

interval field will affect the decreasing rate of D_u. Roughly speaking, when $R_d < 0.5$ the decreasing rates of D_u decrease with the increase of R_d; while the trend is opposite for $R_d > 0.5$. Moreover, the rates of the results have a transition point at around $t = 0.2$ where the decreasing rates shrink significantly. Especially for $R_d \geq 5$, a rebound trend of D_u can be found between $t = 0.2$ and $t = 0.6$. The limit case is the results from the interval variable ('IV' in the figure) model, which corresponds to $R_d \to \infty$ exhibiting a similar trend with the case $R_d > 2$. The authors would like to note that the decrease of D_u with time does not necessarily mean that the uncertainty level is reduced as time progresses, because the deterministic result is also decreasing. To illustrate this point, the upper and lower bounds of the interval field model in Fig.4 are non-dimensionalised with the deterministic result by using $u^* = u/u_d$, where u_d denotes the deterministic result, and are shown in Fig.6. Five time snapshots at $t = \{0, 0.25, 0.5, 0.75, 1\}$ are taken and only half of the domain is presented because of symmetry. It can be seen that the uncertainty level actually increases rather than decreases with time for the upper bounds, and lower bounds experience fluctuations over time. Besides, at each time instant the uncertainty level is almost spatially uniform except for the points close to the middle position, where the deterministic result is zero.

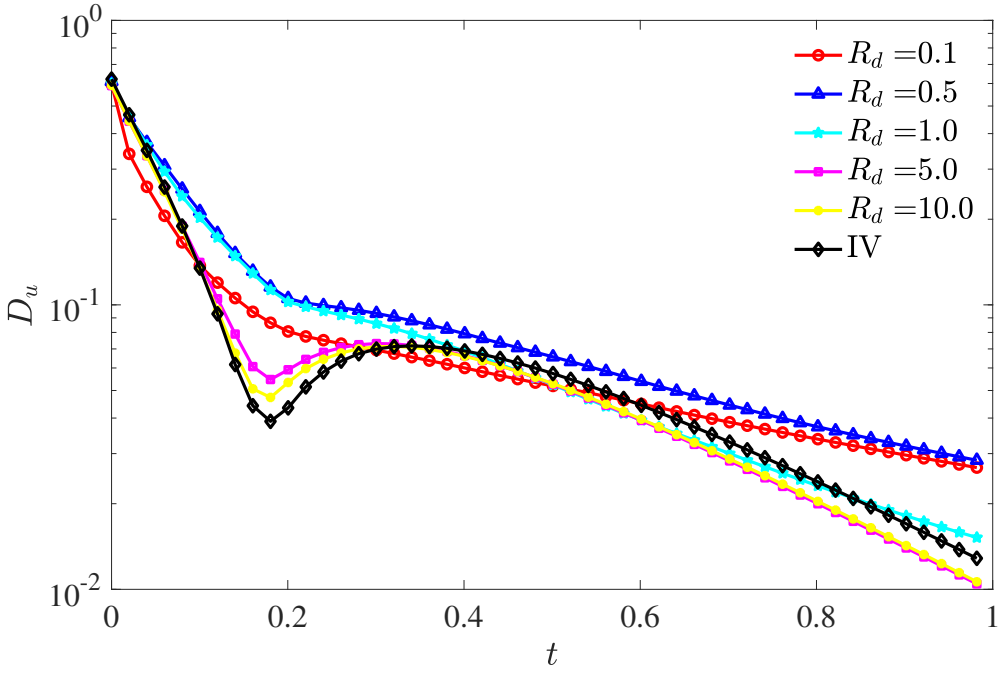

Fig. 5. Difference metric to the deterministic results of the Burgers' equation.

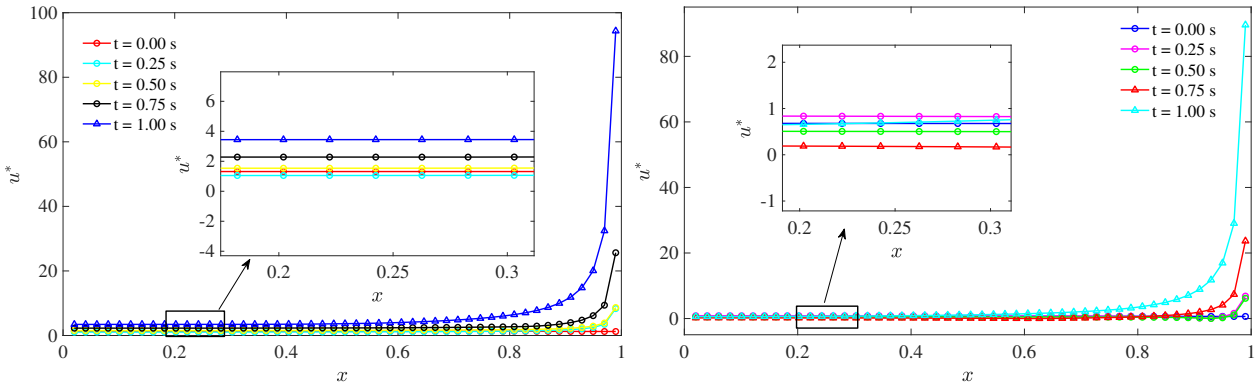

Fig. 6. The non-dimensionlised results for (a) the upper bounds; (b) the lower bounds.

3.3. Euler-Bernoulli beam with spatially varying Young's modulus and external loads

The last case concerns the deformation of a cantilever beam under an external transverse force. Linear elastic material is used. Both Young's modulus and the applied force are considered uncertain quantities and are modelled as interval fields. The governing equation for this problem on the domain $\Omega = [0, L]$ can be written as

$$\frac{\mathrm{d}^2}{\mathrm{d}x^2}[E^{\mathrm{I}}(x, \boldsymbol{\xi})\, I(x) \frac{\mathrm{d}^2 w}{\mathrm{d}x^2}] = p^{\mathrm{I}}(x, \boldsymbol{\eta}),\ x \in \Omega \tag{30}$$

with its boundary conditions (fixed at $x = 0$ and free at $x = L$) as

$$
\begin{aligned}
w(x=0)=0,\ \left.\frac{\mathrm{d}w}{\mathrm{d}x}\right|_{x=0}=0,\\
\left.\frac{\mathrm{d}^2w}{\mathrm{d}x^2}\right|_{x=L}=0,\ -\frac{\mathrm{d}}{\mathrm{d}x}\left[E^{\mathrm{I}}(x,\boldsymbol{\xi})\,I(x)\,\frac{\mathrm{d}^2w}{\mathrm{d}x^2}\right]\Big|_{x=L}=0,
\end{aligned}
\tag{31}
$$

where w is the transverse displacement of the beam, $I(x)$ denotes the moment of inertia of the beam cross section and is assumed to be a constant, e.g. $I(x) = I$. $E^{\mathrm{I}}(x,\boldsymbol{\xi})$ and $p^{\mathrm{I}}(x,\boldsymbol{\eta})$ are respectively the non-deterministic spatially varying Young's modulus and external transverse load, which in this case are modelled as interval fields and are controlled by independent sets of IFCs $\boldsymbol{\xi} = \{\xi_i^{\mathrm{I}}\}_{i=1}^{M}$ and $\boldsymbol{\eta} = \{\eta_i^{\mathrm{I}}\}_{i=1}^{M}$ as

$$
\begin{aligned}
E^{\mathrm{I}}(x,\xi) &= E_c + E_r \sum_{i=1}^{M} B_i(x)\,\xi_i^{\mathrm{I}}\\
p^{\mathrm{I}}(x,\eta) &= p_c + p_r \sum_{i=1}^{M} B_i(x)\,\eta_i^{\mathrm{I}},
\end{aligned}
\tag{32}
$$

where E_c and E_r are the interval centre and interval radius of Young's modulus, similarly, p_c and p_r are those of the external transverse load. $\{B_i(x)\}_{i=1}^{M}$ is a set of cubic B-spline basis functions satisfying partition of unity on Ω, and M is the total number of the B-spline basis functions.

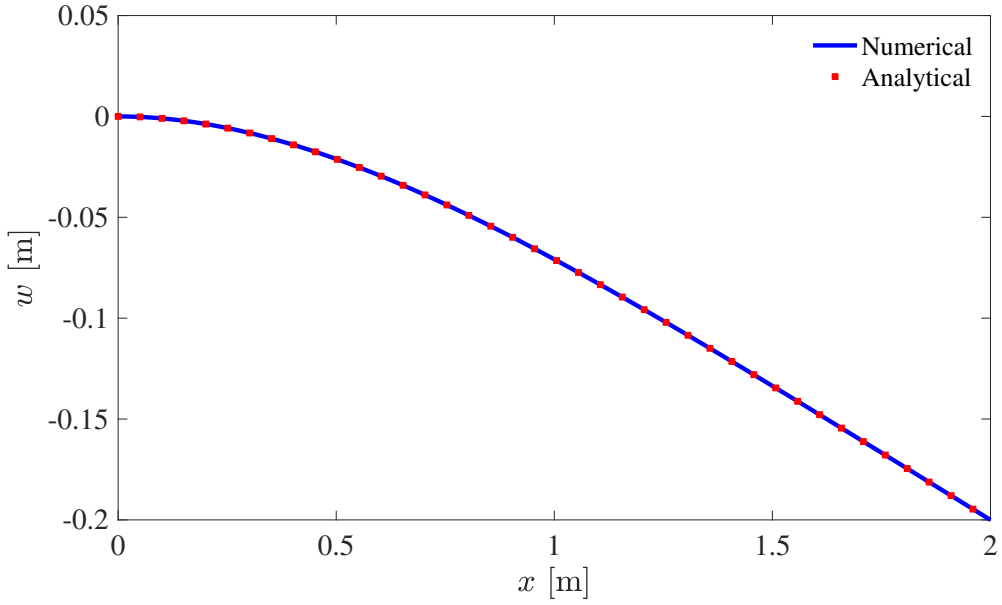

Fig. 7. The numerical result with $E_r = 0,\ p_r = 0$ and the analytical result for the cantilever beam problem.

In order to solve (30) by B-spline collocation method, which is a forth-order differential equation, the approximate solution should be represented by quintic B-spline bases. As performed in the above cases, domain Ω is discretised into N elements with element size h so that $L = Nh$. A new knot vector can be defined as $\hat{\Xi} = [-5h, -4h, \ldots, 0, h, \ldots, Nh, \ldots, (N+4)h, (N+5)h]$, based on which the quintic B-spline

bases $\{\hat{B}_j\}_{j=1}^{N+5}$ are defined. The approximated solution to (30) is obtained as

$$\hat{w}(x) = \sum_{j=1}^{N+5} \hat{B}_j(x)\, w_j, \tag{33}$$

where $\{w_j\}_{j=1}^{N+5}$ are nodal values to be determined. Substitute (32) and (33) into (30), the following expression is obtained as

$$E_r \sum_{i=1}^{M} B_i''(x)\, \xi_i^{\mathrm{I}} I(x) \sum_{j=1}^{N+5} \hat{B}_j''(x)\, w_j + (E_c + E_r \sum_{i=1}^{M} B_i(x)\xi_i^{\mathrm{I}}) \sum_{j=1}^{N+5} \hat{B}_j^{(4)}\, w_j = p_c + p_r \sum_{i=1}^{M} B_i(x)\eta_i^{\mathrm{I}}. \tag{34}$$

Note that in (34), a total number of $N+5$ unknowns are to be solved. The collocation points are set as knots within Ω, i.e. $\{x_j\} = [0, h, 2h, \ldots, (N-1)h, Nh]$. Together with four boundary conditions (31), the problem is ready to be tackled. The procedure to derive the nodal values $\{w_j\}_{j=1}^{N+5}$ is much like the ones that have been described in the last two cases and will not be repeated here.

A numerical case is analysed using the following parameters: $E_c = 10$, $p_c = 1$, $L = 2$, $R_d = 0.5$ and $I = 1$. Firstly, to check the correctness of the method in a deterministic context, let $E_r = 0$ and $p_r = 0$ so the uncertainties are eliminated from the system turning the non-deterministic problem into a deterministic one. The result is compared with the analytical result below

$$w(x) = -\frac{p_c}{24E_cI} x^2(x^2 - 4Lx + 6L^2), \tag{35}$$

and is shown in Fig.7. The numerical results agree with the analytical result, indicating that the B-spline basis functions can represent the spatially varying solution with good accuracy.

Secondly, keep $E_r = 0$ and set $p_r = 0.1p_c$, in which case only the external transverse load is considered non-deterministic. The result is compared with the case in which only the Young's modulus is considered non-deterministic where $E_r = 0.1E_c$ and $p_r = 0$, as shown in Fig.8(a) and (b). The results of the case where both p and E are considered non-deterministic (i.e. $p_r = 0.1p_c$ and $E_r = 0.1E_c$) are shown in Fig.8(c). Besides, in each figure the resulting bounds with the non-deterministic quantities modelled as interval variables are also presented for comparison. It is observed that the results show no noticeable difference between modelling p as an interval field or as an interval variable when p is the only non-deterministic quantity. However, the resulting bounds of the interval field modelling of E are obviously wider than those of the interval variable modelling. The reason for that lies in the fact that the gradient of the interval field of E takes part in the procedure solving the governing equation, as shown in (34), while the information related with the interval field of the external transverse load only appears at the right hand side of the equation.

4. Interval field finite element method

4.1. Interval field finite element formulation

As a complement to the previous sections, the interval field finite element method (IFFEM) is discussed in this section by incorporating the BIFD interval field formulation into solving a FEM problem. A 2D

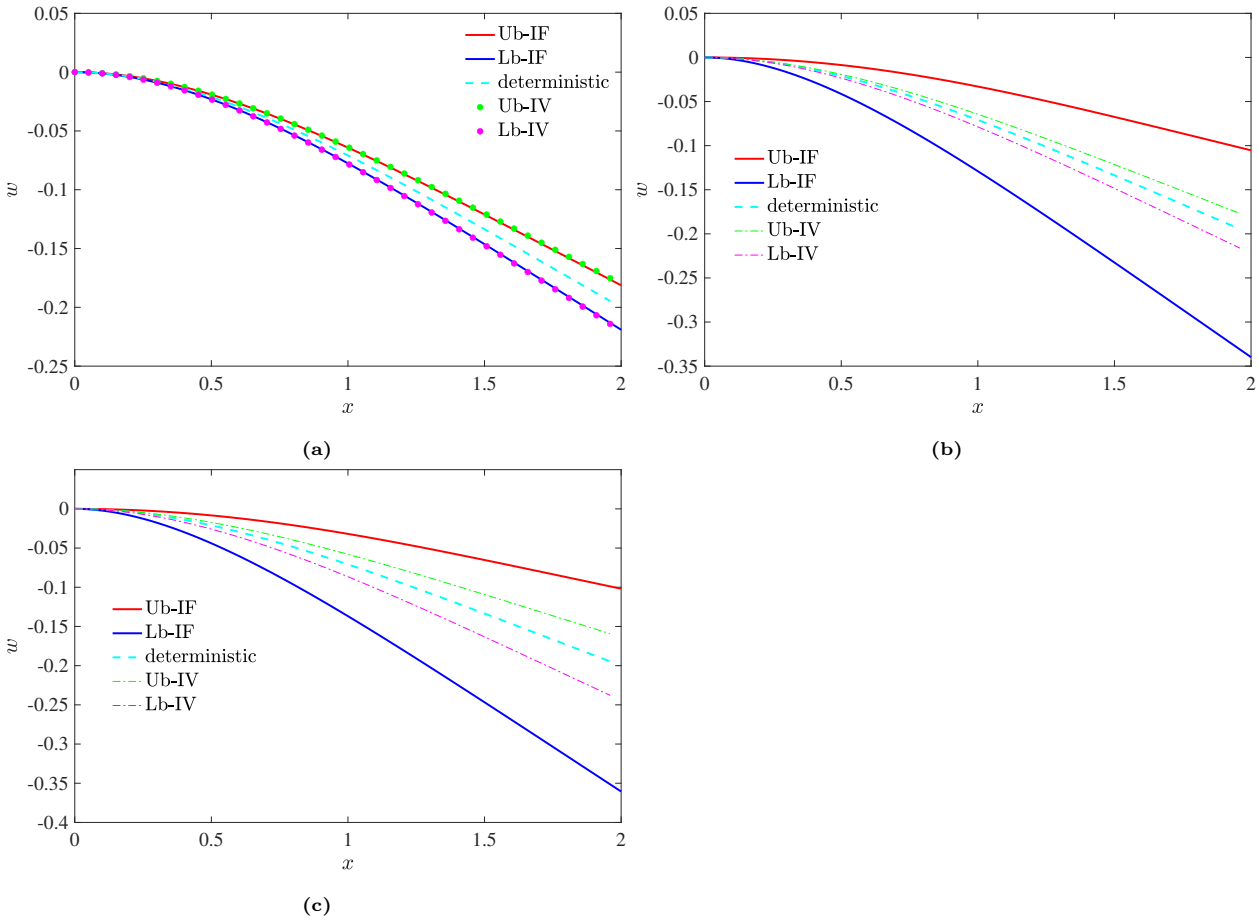

Fig. 8. (a) Results bounds with only p considered non-deterministic; (b) result bounds with only E considered non-deterministic; (c) result bounds with both p and E considered non-deterministic.

numerical case will be presented to demonstrate the application of the method. For a typical linear elastic FEM problem, the domain of interest Ω can be discretised by several finite elements, e.g. $\Omega = \bigcup_{i\in I} \Omega_i$ where I denotes the set of all element indices. The equilibrium equation of an element can be constructed as

$$\mathbf{K}_\mathrm{e}\mathbf{u}_\mathrm{e} = \mathbf{F}_\mathrm{e}, \tag{36}$$

where $\mathbf{u}_\mathrm{e}$ is the element-based vector of nodal displacements, $\mathbf{F}_\mathrm{e}$ is the element-based vector of nodal force. $\mathbf{K}_\mathrm{e}$ is the elemental stiffness matrix that has the form of

$$\mathbf{K}_\mathrm{e} = \int_{\Omega_\mathrm{e}} \mathbf{B}^\mathrm{T}\mathbf{D}\mathbf{B}\, t \,\mathrm{d}\Omega, \tag{37}$$

where $\mathbf{B}$ is the strain-displacement matrix, t is the thickness and $\mathbf{D}$ is the elasticity matrix comprised of material parameters such as the Young's modulus E and Poisson's ratio ν. In the non-deterministic setting, the uncertainties in the material properties can be taken into account, making $\mathbf{D}$ a non-deterministic matrix. For instance, an interval field model of Young's modulus with an interval centre E_c, interval radius E_r and

influence radius R_d has the form of

$$\mathbb{E}^{\mathrm{I}}(\mathbf{x},\boldsymbol{\xi}) = E_c + E_r \sum_{i}^{m} B_i(\mathbf{x})\,\xi_i^{\mathrm{I}},\ \mathbf{x}\in\Omega, \tag{38}$$

where $\mathbb{E}^{\mathrm{I}}(\mathbf{x},\boldsymbol{\xi})$ is expanded by second order 2D B-splines basis functions $\{B_i(\mathbf{x})\}_{i=1}^{m}$ that have support in Ω and are controlled by the influence radius, and $\boldsymbol{\xi} = \{\xi_i^{\mathrm{I}}\}_{i=1}^{m}$ are IFCs. Ensure the mesh size h satisfies $h \le R_d/2$ to capture the local fluctuations in Young's modulus. Under these conditions, the elasticity matrix becomes non-deterministic. Assuming the problem is in the plane stress condition, the explicit expression of the non-deterministic elasticity matrix can be represented as

$$\mathbf{D}^{\mathrm{I}}(\mathbf{x},\boldsymbol{\xi}) = \mathbb{E}^{\mathrm{I}}(\mathbf{x},\boldsymbol{\xi})\,\hat{\mathbf{D}} = \mathbf{D}_0 + \sum_{i=1}^{m} \mathbf{D}_i\,\xi_i^{\mathrm{I}}, \tag{39}$$

with

$$\hat{\mathbf{D}} = \frac{1}{1-\nu^2}\begin{bmatrix} 1 & \nu & 0 \\ \nu & 1 & 0 \\ 0 & 0 & (1-\nu)/2 \end{bmatrix},\ \mathbf{D}_0 = E_c\,\hat{\mathbf{D}},\ \mathbf{D}_i = E_r B_i(\mathbf{x})\,\hat{\mathbf{D}}$$

Consequently, the element stiffness matrix can be expressed as

$$\mathbf{K}_{\mathrm{e}}^{\mathrm{I}}(\mathbf{x},\boldsymbol{\xi}^{\mathrm{I}}) = \int_{\Omega_{\mathrm{e}}} \mathbf{B}^{\mathrm{T}}\mathbf{D}^{\mathrm{I}}(\mathbf{x},\boldsymbol{\xi})\mathbf{B}\,t\,\mathrm{d}\Omega = \mathbf{K}_{0,\mathrm{e}} + \sum_{i=1}^{m} \mathbf{K}_{i,\mathrm{e}}\,\xi_i^{\mathrm{I}}, \tag{40}$$

with

$$\mathbf{K}_{0,e} = \int_{\Omega_{\mathrm{e}}} \mathbf{B}^{\mathrm{T}}\mathbf{D}_0\mathbf{B}\,t\,\mathrm{d}\Omega,\quad \mathbf{K}_{i,\mathrm{e}} = \int_{\Omega_{\mathrm{e}}} \mathbf{B}^{\mathrm{T}}\mathbf{D}_i\mathbf{B}\,t\,\mathrm{d}\Omega.$$

The global stiffness matrix and force vector can be obtained as

$$\begin{aligned} \mathbf{K}^{\mathrm{I}}(\mathbf{x},\boldsymbol{\xi}) &= \sum_{\mathrm{e}=1}^{n_{\mathrm{e}}} \mathbf{T}_{\mathrm{e}}^{\mathrm{T}}\,\mathbf{K}_{\mathrm{e}}^{\mathrm{I}}(\mathbf{x},\boldsymbol{\xi})\,\mathbf{T}_{\mathrm{e}} = \mathbf{K}_0 + \sum_{i=1}^{m} \mathbf{K}_i\,\xi_i^{\mathrm{I}}, \\ \mathbf{F} &= \sum_{\mathrm{e}=1}^{n_{\mathrm{e}}} \mathbf{T}_{\mathrm{e}}^{\mathrm{T}}\,\mathbf{F}_{\mathrm{e}}\,\mathbf{T}_{\mathrm{e}}, \end{aligned} \tag{41}$$

with

$$\mathbf{K}_0 = \sum_{\mathrm{e}=1}^{n_{\mathrm{e}}} \mathbf{T}_{\mathrm{e}}^{\mathrm{T}}\,\mathbf{K}_{0,\mathrm{e}}\,\mathbf{T}_{\mathrm{e}},\quad \mathbf{K}_i = \sum_{\mathrm{e}=1}^{n_{\mathrm{e}}} \mathbf{T}_{\mathrm{e}}^{\mathrm{T}}\,\mathbf{K}_{i,\mathrm{e}}\,\mathbf{T}_{\mathrm{e}}$$

where $\mathbf{T}_{\mathrm{e}}$ denotes the matrix transforming the local stiffness matrix into the global stiffness matrix and n_{e} is the total number of elements. The equilibrium equation for the system can thus be expressed as

$$\mathbf{K}^{\mathrm{I}}(\mathbf{x},\boldsymbol{\xi})\,\mathbf{u} = (\mathbf{K}_0 + \sum_{i=1}^{m} \mathbf{K}_i\,\xi_i^{\mathrm{I}})\,\mathbf{u} = \mathbf{F}. \tag{42}$$

Note that due to the interval matrix $\mathbf{K}^{\mathrm{I}}(\mathbf{x},\boldsymbol{\xi})$ the displacement vector to be sought also becomes an interval vector, e.g. $\mathbf{u} = \mathbf{u}^{\mathrm{I}}(\mathbf{x},\boldsymbol{\xi}) = (\mathbf{K}_0 + \sum_{i=1}^{m} \mathbf{K}_i\,\xi_i^{\mathrm{I}})^{-1}\mathbf{F}$. In most cases, the direct solution to this problem is not available due to the inversion term and thus approximate methods or the MC approach are often used

instead. In what follows, the Neumann expansion method [34, 35] is used to approximate the bounds of the output. The Neumann expansion allows us to represent the inversion term as

$$\begin{aligned}(\mathbf{K}_0+\sum_{i=1}^{m}\mathbf{K}_i\,\xi_i^{\mathrm{I}})^{-1} &= (\mathbf{I}+\sum_{i=1}^{m}\mathbf{K}_0^{-1}\mathbf{K}_i\,\xi_i^{\mathrm{I}})^{-1}\mathbf{K}_0^{-1}\\ &\approx \big[\mathbf{I}-\sum_{i=1}^{m}\mathbf{K}_0^{-1}\mathbf{K}_i\,\xi_i^{\mathrm{I}}+(-1)^2(\sum_{i=1}^{m}\mathbf{K}_0^{-1}\mathbf{K}_i\,\xi_i^{\mathrm{I}})^2+\cdots+(-1)^n(\sum_{i=1}^{m}\mathbf{K}_0^{-1}\mathbf{K}_i\,\xi_i^{\mathrm{I}})^n\big]\mathbf{K}_0^{-1},\end{aligned} \tag{43}$$

where n is the truncation order. The convergence can be guaranteed provided the following condition is satisfied as

$$\rho\Big(\sum_{i=1}^{m}\mathbf{K}_0^{-1}\mathbf{K}_i\,\xi_i^{\mathrm{I}}\Big)\le 1, \tag{44}$$

where $\rho(\cdot)$ denotes the spectral radius. The error of the Neumann expansion can be obtained as

$$\begin{aligned}e &= \|(\mathbf{K}_0+\sum_{i=1}^{m}\mathbf{K}_i\,\xi_i^{\mathrm{I}})^{-1}-\big[\mathbf{I}-\sum_{i=1}^{m}\mathbf{K}_0^{-1}\mathbf{K}_i\,\xi_i^{\mathrm{I}}+\cdots+(-1)^n(\sum_{i=1}^{m}\mathbf{K}_0^{-1}\mathbf{K}_i\,\xi_i^{\mathrm{I}})^n\big]\mathbf{K}_0^{-1}\|_2\\ &= \|(-1)^{n+1}(\sum_{i=1}^{m}\mathbf{K}_0^{-1}\mathbf{K}_i\,\xi_i^{\mathrm{I}})^{n+1}(\mathbf{K}_0+\sum_{i=1}^{m}\mathbf{K}_i\,\xi_i^{\mathrm{I}})^{-1}\|_2\\ &\le \|(\sum_{i=1}^{m}\mathbf{K}_0^{-1}\mathbf{K}_i\,\xi_i^{\mathrm{I}})^{n+1}\|_2\;\|(\mathbf{K}_0+\sum_{i=1}^{m}\mathbf{K}_i\,\xi_i^{\mathrm{I}})^{-1}\|_2.\end{aligned} \tag{45}$$

In light of (44), a sufficient but not necessary condition for the convergence of the Neumann expansion can be expressed as

$$\|\sum_{i=1}^{m}\mathbf{K}_0^{-1}\mathbf{K}_i\|_2<1 \tag{46}$$

With such a condition satisfied, the error will reduce as the number of the truncated terms increases. Denoting $\mathbf{u}_0=\mathbf{K}_0^{-1}\mathbf{F}$, the displacement can be represented as

$$\begin{aligned}\mathbf{u} &\approx \mathbf{u}_0-\sum_{i=1}^{m}\mathbf{K}_0^{-1}\mathbf{K}_i\,\xi_i^{\mathrm{I}}\mathbf{u}_0+(-1)^2(\sum_{i=1}^{m}\mathbf{K}_0^{-1}\mathbf{K}_i\,\xi_i^{\mathrm{I}})^2\mathbf{u}_0+\cdots+(-1)^n(\sum_{i=1}^{m}\mathbf{K}_0^{-1}\mathbf{K}_i\,\xi_i^{\mathrm{I}})^n\mathbf{u}_0\\ &\approx \mathbf{u}_0-\sum_{i=1}^{m}\mathbf{K}_0^{-1}\mathbf{K}_i\,\xi_i^{\mathrm{I}}\mathbf{u}_0.\end{aligned} \tag{47}$$

The second line of (47) represents the approximation of the displacement by keeping only the first-order component, which is generally a good approximation in practical engineering problems when the uncertainty level is not prominent. In this case, the upper and lower bounds of the displacement can be analytically obtained as

$$\begin{cases}\mathbf{u}^{\mathrm{U}}=\mathbf{u}_0+\sum_{i=1}^{m}|\mathbf{K}_0^{-1}\mathbf{K}_i\,\mathbf{u}_0|\\ \mathbf{u}^{\mathrm{L}}=\mathbf{u}_0-\sum_{i=1}^{m}|\mathbf{K}_0^{-1}\mathbf{K}_i\,\mathbf{u}_0|\end{cases} \tag{48}$$

The interval stress analysis can be conducted similarly. Consider the elemental stress $\boldsymbol{\sigma}_{\mathrm{e}}=[\sigma_{\mathrm{e,xx}},\sigma_{\mathrm{e,yy}},\gamma_{\mathrm{e,xy}}]^{\mathrm{T}}$ expressed as

$$\boldsymbol{\sigma}_{\mathrm{e}}=\mathbf{D}^{\mathrm{I}}(\mathbf{x},\boldsymbol{\xi})\mathbf{B}\mathbf{T}_{\mathrm{e}}\mathbf{u} \tag{49}$$

Substituting (39) and $(47)_2$ into (49), the approximate elemental stress can be derived as

$$\begin{aligned}\boldsymbol{\sigma}_{\mathrm{e}} &\approx \big(\mathbf{D}_0+\sum_{i=1}^{m}\mathbf{D}_i\,\xi_i^{\mathrm{I}}\big)\mathbf{B}\mathbf{T}_{\mathrm{e}}\big(\mathbf{u}_0-\sum_{i=1}^{m}\mathbf{K}_0^{-1}\mathbf{K}_i\,\xi_i^{\mathrm{I}}\mathbf{u}_0\big)\\ &=\mathbf{D}_0\mathbf{B}\mathbf{T}_{\mathrm{e}}\mathbf{u}_0+\sum_{i=1}^{m}\big(\mathbf{D}_i\mathbf{B}\mathbf{T}_{\mathrm{e}}\mathbf{u}_0-\mathbf{D}_0\mathbf{B}\mathbf{T}_{\mathrm{e}}\mathbf{K}_0^{-1}\mathbf{K}_i\mathbf{u}_0\big)\xi_i^{\mathrm{I}}+\delta_{\xi\xi},\end{aligned}\tag{50}$$

where $\delta_{\xi\xi}=-\big(\sum_{i=1}^{m}\mathbf{D}_i\xi_i^{\mathrm{I}}\big)\mathbf{B}\mathbf{T}_{\mathrm{e}}\big(\sum_{i=1}^{m}\mathbf{K}_0^{-1}\mathbf{K}_i\,\xi_i^{\mathrm{I}}\mathbf{u}_0\big)$. The elemental stress will have a linear relationship with $\boldsymbol{\xi}$ if further neglecting the term $\delta_{\xi\xi}$, so that its bounds can be approximated as

$$\begin{cases}\boldsymbol{\sigma}_{\mathrm{e}}^{\mathrm{U}}\approx\mathbf{D}_0\mathbf{B}\mathbf{T}_{\mathrm{e}}\mathbf{u}_0+\sum_{i=1}^{m}|\mathbf{D}_i\mathbf{B}\mathbf{T}_{\mathrm{e}}\mathbf{u}_0-\mathbf{D}_0\mathbf{B}\mathbf{T}_{\mathrm{e}}\mathbf{K}_0^{-1}\mathbf{K}_i\mathbf{u}_0|\\ \boldsymbol{\sigma}_{\mathrm{e}}^{\mathrm{L}}\approx\mathbf{D}_0\mathbf{B}\mathbf{T}_{\mathrm{e}}\mathbf{u}_0-\sum_{i=1}^{m}|\mathbf{D}_i\mathbf{B}\mathbf{T}_{\mathrm{e}}\mathbf{u}_0-\mathbf{D}_0\mathbf{B}\mathbf{T}_{\mathrm{e}}\mathbf{K}_0^{-1}\mathbf{K}_i\mathbf{u}_0|.\end{cases}\tag{51}$$

When the uncertainty level is substantial, the first-order approximation of the Neumann expansion may not be accurate enough for predicting the bounds of the output variables. In this case, more terms in the Neumann expansion should be kept to improve accuracy. Denoting $\mathbf{u}_{(n)}=\big[\mathbf{I}-\sum_{i=1}^{m}\mathbf{K}_0^{-1}\mathbf{K}_i\,\xi_i^{\mathrm{I}}+(-1)^2(\sum_{i=1}^{m}\mathbf{K}_0^{-1}\mathbf{K}_i\,\xi_i^{\mathrm{I}})^2+\cdots+(-1)^n(\sum_{i=1}^{m}\mathbf{K}_0^{-1}\mathbf{K}_i\,\xi_i^{\mathrm{I}})^n\big]\mathbf{u}_0$ as the n-th order approximation of the displacement vector. The upper and lower bounds of the j-th components of the displacement vector, denoted as $\mathbf{u}_{(n)j}$, can be obtained through solving the following optimisation problem stated as

$$\begin{aligned}&\text{obj. min } \mathbf{u}_{(n)j}\ \&\max\ \mathbf{u}_{(n)j}\\ &\text{s.t. } \xi_i\in[-1,1],\ i=1,2,\ldots,m.\end{aligned}\tag{52}$$

The solution of the optimisation problem (52) can be determined via a suitable non-linear optimisation solver. After obtaining the solutions for both cases, the upper and lower bounds for $\mathbf{u}_{(n)j}$ can be expressed as

$$\begin{cases}\mathbf{u}_{(n)j}^{\mathrm{U}}=\mathbf{P}_j^{\mathrm{T}}\big[\mathbf{I}-\sum_{i=1}^{m}\mathbf{K}_0^{-1}\mathbf{K}_i\,\xi_i^{\mathrm{U}}+(-1)^2(\sum_{i=1}^{m}\mathbf{K}_0^{-1}\mathbf{K}_i\,\xi_i^{\mathrm{U}})^2+\cdots+(-1)^n(\sum_{i=1}^{m}\mathbf{K}_0^{-1}\mathbf{K}_i\,\xi_i^{\mathrm{U}})^n\big]\mathbf{u}_0,\\ \mathbf{u}_{(n)j}^{\mathrm{L}}=\mathbf{P}_j^{\mathrm{T}}\big[\mathbf{I}-\sum_{i=1}^{m}\mathbf{K}_0^{-1}\mathbf{K}_i\,\xi_i^{\mathrm{L}}+(-1)^2(\sum_{i=1}^{m}\mathbf{K}_0^{-1}\mathbf{K}_i\,\xi_i^{\mathrm{L}})^2+\cdots+(-1)^n(\sum_{i=1}^{m}\mathbf{K}_0^{-1}\mathbf{K}_i\,\xi_i^{\mathrm{L}})^n\big]\mathbf{u}_0,\end{cases}\tag{53}$$

where $\{\xi_i^{\mathrm{U}}\}$ and $\{\xi_i^{\mathrm{L}}\}$ indicate the optimal solutions for the maximisation and minimisation problems, respectively, and $\mathbf{P}_j$ is a $\#\mathrm{dof}\times 1$ vector used to pick up the j-th component of the displacement vector with its j-th component being 1 and all other components being zero. Similarly, the n-th order approximation of the elemental stress vector can be expressed as

$$\boldsymbol{\sigma}_{\mathrm{e}}^{(n)}=\big(\mathbf{D}_0+\sum_{i=1}^{m}\mathbf{D}_i\,\xi_i^{\mathrm{I}}\big)\mathbf{B}\mathbf{T}_{\mathrm{e}}\big[\mathbf{I}+(-1)\sum_{i=1}^{m}\mathbf{K}_0^{-1}\mathbf{K}_i\,\xi_i^{\mathrm{I}}+\cdots+(-1)^n(\sum_{i=1}^{m}\mathbf{K}_0^{-1}\mathbf{K}_i\,\xi_i^{\mathrm{I}})^n\big]\mathbf{u}_0.\tag{54}$$

The optimisation problem for solving the bounds of the j-th component of the elemental stress vector can be stated as

$$\begin{aligned}&\text{obj. min } \boldsymbol{\sigma}_{\mathrm{e}j}^{(n)}\ \&\max\ \boldsymbol{\sigma}_{\mathrm{e}j}^{(n)}\\ &\text{s.t. } \xi_i\in[-1,1],\ i=1,2,\ldots,m.\end{aligned}\tag{55}$$

The resulting bounds for $\boldsymbol{\sigma}_{\mathrm{e}j}^{(n)}$ can be expressed as

$$\begin{cases} \boldsymbol{\sigma}_{\mathrm{e}j}^{\mathrm{U}(n)} = \mathbf{Q}_j^{\mathrm{T}}\big(\mathbf{D}_0 + \sum_{i=1}^{m} \mathbf{D}_i\, \hat{\xi}_i^{\mathrm{U}}\big)\mathbf{B}\mathbf{T}_{\mathrm{e}}\big[\mathbf{I} + (-1)\sum_{i=1}^{m} \mathbf{K}_0^{-1}\mathbf{K}_i\, \hat{\xi}_i^{\mathrm{U}} + \cdots + (-1)^n(\sum_{i=1}^{m} \mathbf{K}_0^{-1}\mathbf{K}_i\, \hat{\xi}_i^{\mathrm{U}})^n\big]\mathbf{u}_0, \\ \boldsymbol{\sigma}_{\mathrm{e}j}^{\mathrm{L}(n)} = \mathbf{Q}_j^{\mathrm{T}}\big(\mathbf{D}_0 + \sum_{i=1}^{m} \mathbf{D}_i\, \hat{\xi}_i^{\mathrm{L}}\big)\mathbf{B}\mathbf{T}_{\mathrm{e}}\big[\mathbf{I} + (-1)\sum_{i=1}^{m} \mathbf{K}_0^{-1}\mathbf{K}_i\, \hat{\xi}_i^{\mathrm{L}} + \cdots + (-1)^n(\sum_{i=1}^{m} \mathbf{K}_0^{-1}\mathbf{K}_i\, \hat{\xi}_i^{\mathrm{L}})^n\big]\mathbf{u}_0, \end{cases} \tag{56}$$

where $\{\hat{\xi}_i^{\mathrm{U}}\}$ and $\{\hat{\xi}_i^{\mathrm{L}}\}$ indicate the optimal solutions for the maximisation and minimisation problems, respectively. $\mathbf{Q}_j$ is a 3×1 vector with the j-th component being 1 and others being zero.

4.2. Numerical case: square plane

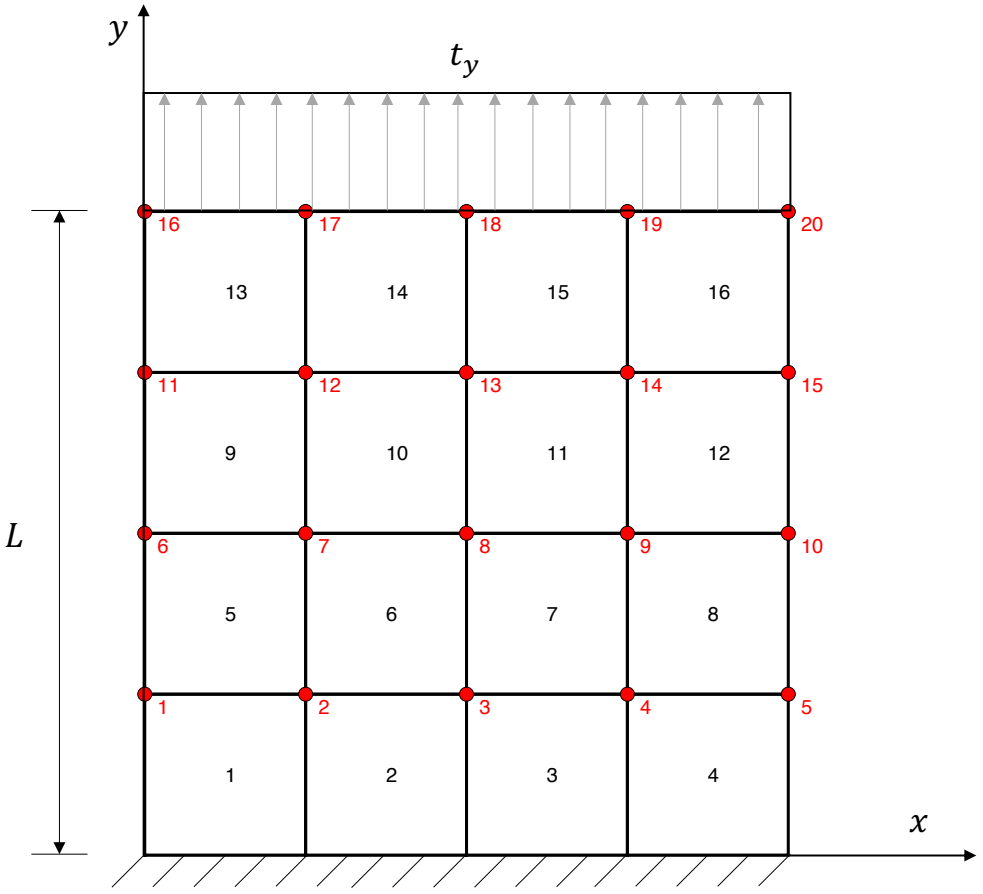

Fig. 9. The square plane setting.

A linear elastic square plane with uncertain Young's modulus and uniform traction on its top edge will be presented as a demonstrative case, as shown in Fig.9. The bottom edge of the plane is fixed and the thickness is t. The plane geometry is meshed into 16 equally sized elements with in total 25 nodes (20 nodes are active and marked red). The Young's modulus of the plane is characterised by an interval field with interval centre E_c, interval radius E_r and influence radius R_d. The parameters used in this case are collected into Table 2. Two realisations of the Young's modulus interval field has been depicted in Fig.10.

Table 2: Parameters for the square plane

L [m]	E_c [Pa]	E_r [Pa]	ν	R_d [m]	t_y [Pa]	t [m]
1	2×10^{11}	2×10^{10}	0.3	0.5	1×10^{9}	0.001

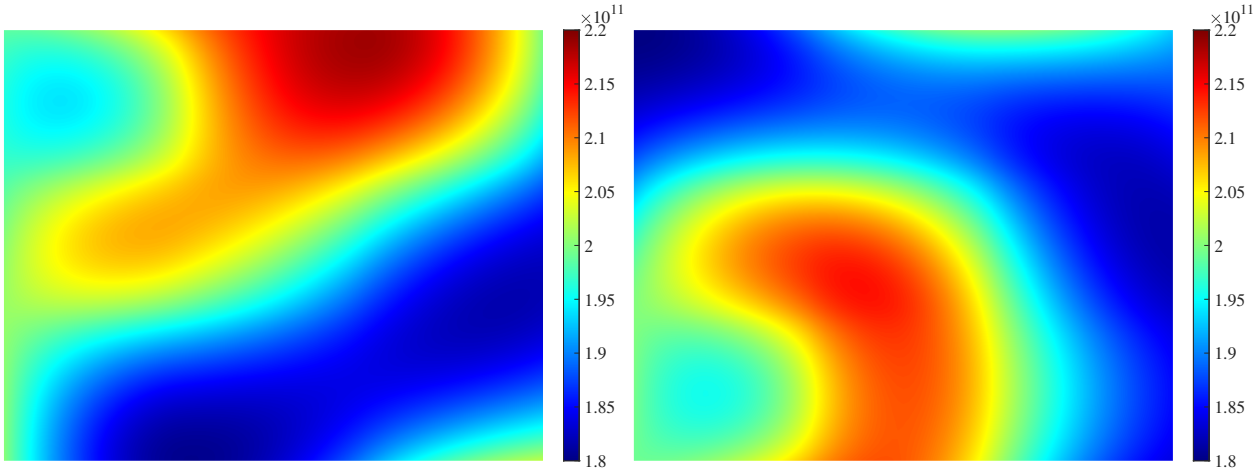

Fig. 10. Two realisations of the Young's modulus interval field.

In the following analysis, the displacements in the y-direction of each active node and the elemental stress in the y-direction of each elements are examined. The convergence condition is satisfied after checking (46), enabling the Neumann expansion method to be employed. Using the Neumann expansion method elaborated in the last subsection, the upper and lower bounds of the displacement and elemental stress can be obtained and are compared with the bounds obtained by the MC approach with 10^6 realisations. The results are presented in Fig.11. It can be observed that for both the displacement and the elemental stress, the bounds obtained by both methods match well. The stress bound curves approximated using the Neumann expansion method make a slightly narrower band than those of the MC approach, resulting in being enclosed by the latter. Furthermore, the results using the Neumann expansion method were obtained 3000 times faster than those using the MC approach, taking only a few seconds to compute.

In a situation where the uncertainty level becomes substantial, e.g. $E_r/E_c > 0.1$, additional terms of the Neumann expansion should be considered to improve accuracy. In Table 3 and 4, three different levels of uncertainty, i.e. $E_r/E_c = \{0.1, 0.3, 0.5\}$ are investigated. The upper and lower bounds of the displacement and stress vectors are approximated by up to 4th order Neumann expansion method and are compared with the corresponding results obtained by MC approach with a sample size of 10^6. The relative error in the L_2 norm are calculated and presented in the tables. It can be observed that the first order approximation for bounds of displacement is satisfactory when $E_r/E_c = 0.1$, whereas on other two uncertainty levels the errors increase significantly. However, the second order approximation can significantly improve the accuracy, keeping the error within 5%. Moreover, the accuracy does not get further improvement when using third

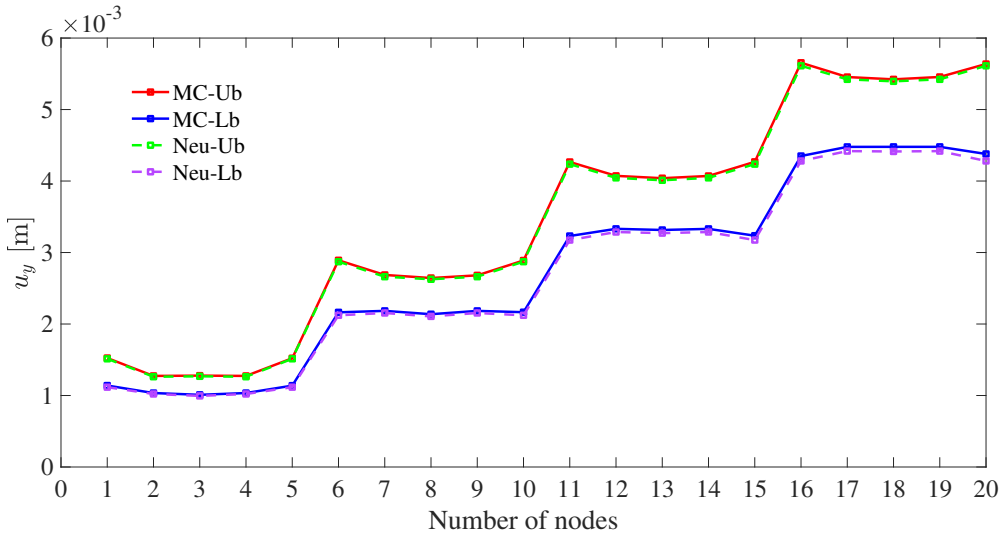

(a)

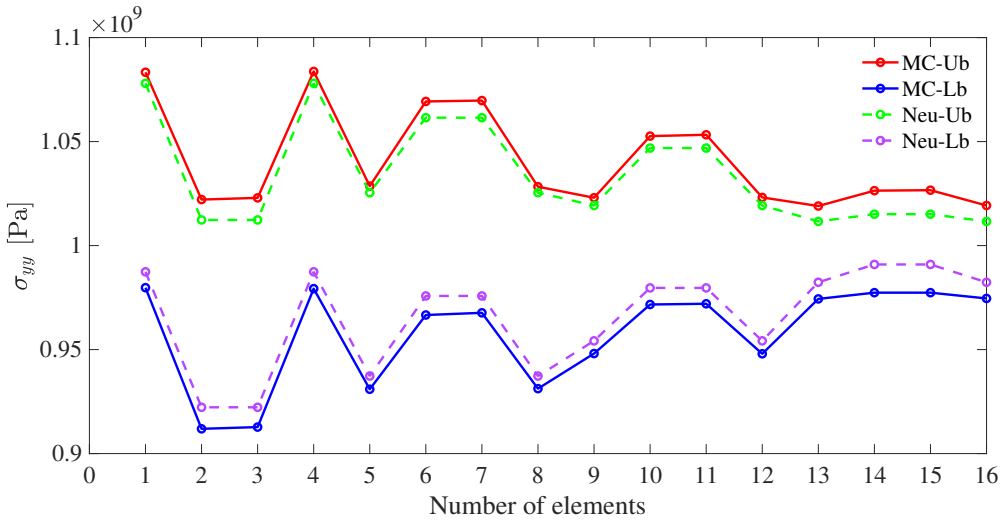

(b)

Fig. 11. (a) Nodal displacement bounds and (b) elemental stress bounds in the y-direction achieved by the Neumann expansion method and the MC approach.

or fourth order approximation. As for predicting the bounds for the stress vector, the first order Neumann approximation can provide results with acceptable accuracy for the first two uncertainty levels. However, in the third case the approximated lower bound has more than 10% relative error compared with that of the MC approach. It can be improved by the second order Neumann approximation. However, it should be noted that since the second order and higher-order approximations require solving element-wise optimisation problems, the efficiency will decrease though it will still be more preferable than the MC approach.

Table 3: Relative error of the displacement vector $\|\mathbf{u}_{\mathrm{Neu}} - \mathbf{u}_{\mathrm{MC}}\|_2/\|\mathbf{u}_{\mathrm{MC}}\|_2$ for various E_r/E_c levels with up to 4th order approximation.

E_r/E_c	1st (%)		2nd (%)		3rd (%)		4th (%)	
	Ub	Lb	Ub	Lb	Ub	Lb	Ub	Lb
0.1	2.15	2.41	0.25	0.34	0.26	0.34	0.26	0.34
0.3	8.14	11.63	1.02	1.19	1.04	1.26	1.05	1.25
0.5	23.67	31.58	1.51	3.26	1.47	2.29	1.46	2.30

Table 4: Relative error of the stress vector $\|\boldsymbol{\sigma}_{\mathrm{Neu}} - \boldsymbol{\sigma}_{\mathrm{MC}}\|_2/\|\boldsymbol{\sigma}_{\mathrm{MC}}\|_2$ for various E_r/E_c levels with up to 4th order approximation.

E_r/E_c	1st (%)		2nd (%)		3rd (%)		4th (%)	
	Ub	Lb	Ub	Lb	Ub	Lb	Ub	Lb
0.1	0.72	0.92	0.77	0.87	0.79	0.88	0.79	0.88
0.3	2.52	3.98	2.37	2.81	2.95	3.16	2.80	3.26
0.5	5.17	10.29	3.90	5.63	7.85	5.06	5.92	6.24

5. Conclusions

This paper presents the uncertainty propagation problem with the uncertain parameters modelled as interval fields by the recently proposed B-spline based interval field decomposition method. The method facilitates a direct incorporation of the interval field formulation into the system's governing equation due to its explicit form. With the solution being approximated by B-spline basis expansion, the governing equation can be solved by the collocation method, thanks to the high-degree continuity of the B-spline basis functions. Three different boundary value problems are investigated and conclusions are drawn as follows.

(1) The simple case of steady-state heat conduction shows the output bounds can be predicted analytically using an optimisation method for small-scale problems. For a large-scale problem, such a method becomes computationally prohibitive and a numerical approach, e.g. Monte-Carlo approach, is necessary;

(2) The problem of Burgers' equation shows that the uncertainties in the output may not decrease with time although the deterministic results decrease. The interval field model yields less conservative results than the interval variable model;

(3) The cantilever beam case reveals that both the variation of the Young's modulus and the external load will affect the deformed configuration of the beam. In the specific settings presented, the impact of the Young's modulus is found to be greater than that of the external load.

Finally, the interval field finite element method is introduced. The bounds of the quantities of interest can be effectively approximated by using the first-order Neumann expansion method, compared with the results obtained by the MC approach, with good accuracy when the uncertainty level is not substantial.

When the uncertainty level is high, second-order approximation should be used to significantly improve the accuracy but with reduced efficiency due to the use of element-wise optimisation techniques.

Acknowledgments

The first author H. Hu gratefully acknowledges the financial support from the University of Liverpool and China Scholarship Council Awards (CSC NO.201906230311).

Appendix A Explicit result to the heat conduction problem

Since in this case $n_c = N + 3 = 5$, the solution to (14) has five components $\{t_i\}_{i=1}^5$ and can be derived as follows

$$
\begin{aligned}
t_1 = &-(1008\xi_2 + 1584\xi_3 + 1872\xi_4 + 720\xi_5 + 318\xi_2\xi_3 + 576\xi_2\xi_4 + 210\xi_2\xi_5 + 666\xi_3\xi_4 + 360\xi_3\xi_5 + 150\xi_4\xi_5 \\
&- 15\xi_2\xi_3^2 + 2\xi_2^2\xi_3 + 80\xi_2\xi_4^2 - 16\xi_2^2\xi_4 + 40\xi_3\xi_4^2 - 10\xi_2^2\xi_5 + 59\xi_3^2\xi_4 + 40\xi_3^2\xi_5 - 48\xi_2^2 + 120\xi_3^2 - 8\xi_3^3 + 240\xi_4^2 \\
&+ 110\xi_2\xi_3\xi_4 + 75\xi_2\xi_3\xi_5 + 50\xi_2\xi_4\xi_5 + 25\xi_3\xi_4\xi_5 + 3456)/(1296\xi_1 + 2880\xi_2 + 2016\xi_3 + 2880\xi_4 + 1296\xi_5 \\
&+ 126\xi_1\xi_2 + 408\xi_1\xi_3 + 522\xi_1\xi_4 + 696\xi_2\xi_3 + 240\xi_1\xi_5 + 1152\xi_2\xi_4 + 522\xi_2\xi_5 + 696\xi_3\xi_4 + 408\xi_3\xi_5 + 126\xi_4\xi_5 \\
&- 8\xi_1\xi_3^2 + 30\xi_1\xi_4^2 - 16\xi_2\xi_3^2 + 2\xi_2^2\xi_3 + 64\xi_2\xi_4^2 + 64\xi_2^2\xi_4 + 2\xi_3\xi_4^2 + 30\xi_2^2\xi_5 - 16\xi_3^2\xi_4 - 8\xi_3^2\xi_5 + 192\xi_2^2 - 96\xi_3^2 \\
&+ 192\xi_4^2 + \xi_1\xi_2\xi_3 + 42\xi_1\xi_2\xi_4 + 20\xi_1\xi_2\xi_5 + 139\xi_1\xi_3\xi_4 + 80\xi_1\xi_3\xi_5 + 236\xi_2\xi_3\xi_4 + 20\xi_1\xi_4\xi_5 + 139\xi_2\xi_3\xi_5 \\
&+ 42\xi_2\xi_4\xi_5 + \xi_3\xi_4\xi_5 + 6912)
\end{aligned}
$$

$$
\begin{aligned}
t_2 = &-\frac{1}{4}(576\xi_1 - 576\xi_3 - 24\xi_1\xi_2 + 168\xi_1\xi_3 + 312\xi_1\xi_4 + 24\xi_2\xi_3 + 120\xi_1\xi_5 - 312\xi_3\xi_4 - 120\xi_3\xi_5 - 8\xi_1\xi_3^2 \\
&+ 40\xi_1\xi_4^2 - \xi_2\xi_3^2 - 40\xi_3\xi_4^2 - 59\xi_3^2\xi_4 - 40\xi_3^2\xi_5 - 168\xi_3^2 + 8\xi_3^3 + \xi_1\xi_2\xi_3 - 8\xi_1\xi_2\xi_4 - 5\xi_1\xi_2\xi_5 + 59\xi_1\xi_3\xi_4 \\
&+ 40\xi_1\xi_3\xi_5 + 8\xi_2\xi_3\xi_4 + 25\xi_1\xi_4\xi_5 + 5\xi_2\xi_3\xi_5 - 25\xi_3\xi_4\xi_5)/(1296\xi_1 + 2880\xi_2 + 2016\xi_3 + 2880\xi_4 + 1296\xi_5 \\
&+ 126\xi_1\xi_2 + 408\xi_1\xi_3 + 522\xi_1\xi_4 + 696\xi_2\xi_3 + 240\xi_1\xi_5 + 1152\xi_2\xi_4 + 522\xi_2\xi_5 + 696\xi_3\xi_4 + 408\xi_3\xi_5 + 126\xi_4\xi_5 \\
&- 8\xi_1\xi_3^2 + 30\xi_1\xi_4^2 - 16\xi_2\xi_3^2 + 2\xi_2^2\xi_3 + 64\xi_2\xi_4^2 + 64\xi_2^2\xi_4 + 2\xi_3\xi_4^2 + 30\xi_2^2\xi_5 - 16\xi_3^2\xi_4 - 8\xi_3^2\xi_5 + 192\xi_2^2 - 96\xi_3^2 \\
&+ 192\xi_4^2 + \xi_1\xi_2\xi_3 + 42\xi_1\xi_2\xi_4 + 20\xi_1\xi_2\xi_5 + 139\xi_1\xi_3\xi_4 + 80\xi_1\xi_3\xi_5 + 236\xi_2\xi_3\xi_4 + 20\xi_1\xi_4\xi_5 + 139\xi_2\xi_3\xi_5 \\
&+ 42\xi_2\xi_4\xi_5 + \xi_3\xi_4\xi_5 + 6912)
\end{aligned}
$$

$$
\begin{aligned}
t_3 = &(576\xi_1 + 1008\xi_2 + 1008\xi_3 + 1872\xi_4 + 720\xi_5 - 24\xi_1\xi_2 + 168\xi_1\xi_3 + 312\xi_1\xi_4 + 342\xi_2\xi_3 + 120\xi_1\xi_5 + 576\xi_2\xi_4 \\
&+ 210\xi_2\xi_5 + 354\xi_3\xi_4 + 240\xi_3\xi_5 + 150\xi_4\xi_5 - 8\xi_1\xi_3^2 + 40\xi_1\xi_4^2 - 16\xi_2\xi_3^2 + 2\xi_2^2\xi_3 + 80\xi_2\xi_4^2 - 16\xi_2^2\xi_4 - 10\xi_2^2\xi_5 \\
&- 48\xi_2^2 - 48\xi_3^2 + 240\xi_4^2 + \xi_1\xi_2\xi_3 - 8\xi_1\xi_2\xi_4 - 5\xi_1\xi_2\xi_5 + 59\xi_1\xi_3\xi_4 + 40\xi_1\xi_3\xi_5 + 118\xi_2\xi_3\xi_4 + 25\xi_1\xi_4\xi_5 + 80\xi_2\xi_3\xi_5 \\
&+ 50\xi_2\xi_4\xi_5 + 3456)/(1296\xi_1 + 2880\xi_2 + 2016\xi_3 + 2880\xi_4 + 1296\xi_5 + 126\xi_1\xi_2 + 408\xi_1\xi_3 + 522\xi_1\xi_4 + 696\xi_2\xi_3 \\
&+ 240\xi_1\xi_5 + 1152\xi_2\xi_4 + 522\xi_2\xi_5 + 696\xi_3\xi_4 + 408\xi_3\xi_5 + 126\xi_4\xi_5 - 8\xi_1\xi_3^2 + 30\xi_1\xi_4^2 - 16\xi_2\xi_3^2 + 2\xi_2^2\xi_3 + 64\xi_2\xi_4^2 \\
&+ 64\xi_2^2\xi_4 + 2\xi_3\xi_4^2 + 30\xi_2^2\xi_5 - 16\xi_3^2\xi_4 - 8\xi_3^2\xi_5 + 192\xi_2^2 - 96\xi_3^2 + 192\xi_4^2 + \xi_1\xi_2\xi_3 + 42\xi_1\xi_2\xi_4 + 20\xi_1\xi_2\xi_5 + 139\xi_1\xi_3\xi_4 \\
&+ 80\xi_1\xi_3\xi_5 + 236\xi_2\xi_3\xi_4 + 20\xi_1\xi_4\xi_5 + 139\xi_2\xi_3\xi_5 + 42\xi_2\xi_4\xi_5 + \xi_3\xi_4\xi_5 + 6912)
\end{aligned}
$$

$$t_4 = ((8\xi_4 - \xi_3 + 5\xi_5 + 24)(216\xi_1 + 480\xi_2 + 360\xi_3 + 96\xi_4 + 21\xi_1\xi_2 + 72\xi_1\xi_3 + 15\xi_1\xi_4 + 123\xi_2\xi_3 + 32\xi_2\xi_4 + \xi_3\xi_4 + 32\xi_2^2 - 8\xi_3^2 + 1152))/(4(1296\xi_1 + 2880\xi_2 + 2016\xi_3 + 2880\xi_4 + 1296\xi_5 + 126\xi_1\xi_2 + 408\xi_1\xi_3 + 522\xi_1\xi_4 + 696\xi_2\xi_3 + 240\xi_1\xi_5 + 1152\xi_2\xi_4 + 522\xi_2\xi_5 + 696\xi_3\xi_4 + 408\xi_3\xi_5 + 126\xi_4\xi_5 - 8\xi_1\xi_3^2 + 30\xi_1\xi_4^2 - 16\xi_2\xi_3^2 + 2\xi_2^2\xi_3 + 64\xi_2\xi_4^2 + 64\xi_2^2\xi_4 + 2\xi_3\xi_4^2 + 30\xi_2^2\xi_5 - 16\xi_3^2\xi_4 - 8\xi_3^2\xi_5 + 192\xi_2^2 - 96\xi_3^2 + 192\xi_4^2 + \xi_1\xi_2\xi_3 + 42\xi_1\xi_2\xi_4 + 20\xi_1\xi_2\xi_5 + 139\xi_1\xi_3\xi_4 + 80\xi_1\xi_3\xi_5 + 236\xi_2\xi_3\xi_4 + 20\xi_1\xi_4\xi_5 + 139\xi_2\xi_3\xi_5 + 42\xi_2\xi_4\xi_5 + \xi_3\xi_4\xi_5 + 6912))$$

$$t_5 = (2016\xi_1 + 4752\xi_2 + 3600\xi_3 + 3888\xi_4 + 1296\xi_5 + 276\xi_1\xi_2 + 768\xi_1\xi_3 + 732\xi_1\xi_4 + 1362\xi_2\xi_3 + 240\xi_1\xi_5 + 1728\xi_2\xi_4 + 522\xi_2\xi_5 + 1014\xi_3\xi_4 + 408\xi_3\xi_5 + 126\xi_4\xi_5 + 32\xi_1\xi_3^2 + 20\xi_1\xi_4^2 + 43\xi_2\xi_3^2 + 42\xi_2^2\xi_3 + 48\xi_2\xi_4^2 + 144\xi_2^2\xi_4 + 4\xi_3\xi_4^2 + 30\xi_2^2\xi_5 - 31\xi_3^2\xi_4 - 8\xi_3^2\xi_5 + 432\xi_2^2 + 24\xi_3^2 - 8\xi_3^3 + 144\xi_4^2 + 26\xi_1\xi_2\xi_3 + 92\xi_1\xi_2\xi_4 + 20\xi_1\xi_2\xi_5 + 214\xi_1\xi_3\xi_4 + 80\xi_1\xi_3\xi_5 + 346\xi_2\xi_3\xi_4 + 20\xi_1\xi_4\xi_5 + 139\xi_2\xi_3\xi_5 + 42\xi_2\xi_4\xi_5 + \xi_3\xi_4\xi_5 + 10368)/(1296\xi_1 + 2880\xi_2 + 2016\xi_3 + 2880\xi_4 + 1296\xi_5 + 126\xi_1\xi_2 + 408\xi_1\xi_3 + 522\xi_1\xi_4 + 696\xi_2\xi_3 + 240\xi_1\xi_5 + 1152\xi_2\xi_4 + 522\xi_2\xi_5 + 696\xi_3\xi_4 + 408\xi_3\xi_5 + 126\xi_4\xi_5 - 8\xi_1\xi_3^2 + 30\xi_1\xi_4^2 - 16\xi_2\xi_3^2 + 2\xi_2^2\xi_3 + 64\xi_2\xi_4^2 + 64\xi_2^2\xi_4 + 2\xi_3\xi_4^2 + 30\xi_2^2\xi_5 - 16\xi_3^2\xi_4 - 8\xi_3^2\xi_5 + 192\xi_2^2 - 96\xi_3^2 + 192\xi_4^2 + \xi_1\xi_2\xi_3 + 42\xi_1\xi_2\xi_4 + 20\xi_1\xi_2\xi_5 + 139\xi_1\xi_3\xi_4 + 80\xi_1\xi_3\xi_5 + 236\xi_2\xi_3\xi_4 + 20\xi_1\xi_4\xi_5 + 139\xi_2\xi_3\xi_5 + 42\xi_2\xi_4\xi_5 + \xi_3\xi_4\xi_5 + 6912)$$

References

[1] I. Elishakoff, Probabilistic methods in the theory of structures: strength of materials, random vibrations, and random buckling, World Scientific, 2017. doi:http://dx.doi.org/10.1142/10274.

[2] G. Stefanou, The stochastic finite element method: past, present and future, Computer methods in applied mechanics and engineering 198 (9-12) (2009) 1031–1051. doi:http://dx.doi.org/10.1016/j.cma.2008.11.007.

[3] I. Elishakoff, P. Elisseeff, S. A. Glegg, Nonprobabilistic, convex-theoretic modeling of scatter in material properties, AIAA journal 32 (4) (1994) 843–849. doi:http://dx.doi.org/10.2514/3.12062.

[4] I. Elishakoff, Possible limitations of probabilistic methods in engineering, Applied Mechanics Reviews 53 (2) (2000). doi:http://dx.doi.org/10.1115/1.3097337.

[5] L. Jaulin, M. Kieffer, O. Didrit, E. Walter, Interval analysis, in: Applied interval analysis, Springer, 2001, pp. 11–43. doi:https://doi.org/10.1007/978-1-4471-0249-6.

[6] R. E. Moore, Methods and applications of interval analysis, SIAM, 1979. doi:http://dx.doi.org/10.1137/1.9781611970906.

[7] J. Jakeman, M. Eldred, D. Xiu, Numerical approach for quantification of epistemic uncertainty, Journal of Computational Physics 229 (12) (2010) 4648–4663. doi:http://dx.doi.org/10.1016/j.jcp.2010.03.003.

[8] H.-J. Zimmermann, Fuzzy set theory—and its applications, Springer Science & Business Media, 2011. doi:https://doi.org/10.1007/978-94-015-7949-0.

[9] C. Kahraman, B. Öztayşi, S. Çevik Onar, A comprehensive literature review of 50 years of fuzzy set theory, International Journal of Computational Intelligence Systems 9 (sup1) (2016) 3–24. doi:http://dx.doi.org/10.1080/18756891.2016.1180817.

[10] J. A. Barnett, Computational methods for a mathematical theory of evidence, in: Classic Works of the Dempster-Shafer Theory of Belief Functions, Springer, 2008, pp. 197–216. doi:https://doi.org/10.1007/978-3-540-44792-4_8.

[11] H. Agarwal, J. E. Renaud, E. L. Preston, D. Padmanabhan, Uncertainty quantification using evidence theory in multidisciplinary design optimization, Reliability Engineering & System Safety 85 (1-3) (2004) 281–294. doi:http://dx.doi.org/10.1016/j.ress.2004.03.017.

[12] W. Dong, H. C. Shah, Vertex method for computing functions of fuzzy variables, Fuzzy Sets and Systems 24 (1) (1987) 65–78. doi:https://doi.org/10.1016/0165-0114(87)90114-X.
URL https://www.sciencedirect.com/science/article/pii/016501148790114X

[13] D. Dubois, H. Fargier, J. Fortin, A generalized vertex method for computing with fuzzy intervals, in: 2004 IEEE International Conference on Fuzzy Systems (IEEE Cat. No. 04CH37542), Vol. 1, IEEE, 2004, pp. 541–546. doi:http://dx.doi.org/10.1109/FUZZY.2004.1375793.

[14] R. E. Moore, R. B. Kearfott, M. J. Cloud, Introduction to interval analysis, SIAM, 2009. doi:10.1137/1.9780898717716.ch1.

[15] D. Moens, M. De Munck, W. Desmet, D. Vandepitte, Numerical dynamic analysis of uncertain mechanical structures based on interval fields, in: IUTAM symposium on the vibration analysis of structures with uncertainties, Springer, 2011, pp. 71–83. doi:https://doi.org/10.1007/978-94-007-0289-9_6.

[16] C. van Mierlo, M. G. Faes, D. Moens, Inhomogeneous interval fields based on scaled inverse distance weighting interpolation, Computer Methods in Applied Mechanics and Engineering 373 (2021) 113542. doi:https://doi.org/10.1016/j.cma.2020.113542.

[17] R. R. Callens, M. G. Faes, D. Moens, Local explicit interval fields for non-stationary uncertainty modelling in finite element models, Computer Methods in Applied Mechanics and Engineering 379 (2021) 113735. doi:https://doi.org/10.1016/j.cma.2021.113735.

[18] M. Imholz, D. Vandepitte, D. Moens, Derivation of an input interval field decomposition based on expert knowledge using locally defined basis functions, in: UNCECOMP 2015-1st ECCOMAS Thematic Conference on Uncertainty Quantification in Computational Sciences and Engineering, 2015, pp. 529–547. doi:https://doi.org/10.7712/120215.4290.583.

[19] H. Hu, Y. Wu, A. Batou, H. Ouyang, B-spline based interval field decomposition method, Computers & Structures 272 (2022) 106874. doi:10.1016/j.compstruc.2022.106874.

[20] A. Sofi, Structural response variability under spatially dependent uncertainty: stochastic versus interval model, Probabilistic Engineering Mechanics 42 (2015) 78–86. doi:https://doi.org/10.1016/j.probengmech.2015.09.001.

[21] A. Sofi, E. Romeo, O. Barrera, A. Cocks, An interval finite element method for the analysis of structures with spatially varying uncertainties, Advances in Engineering Software 128 (2019) 1–19. doi:https://doi.org/10.1016/j.advengsoft.2018.11.001.

[22] C. Jiang, B. Ni, X. Han, Y. Tao, Non-probabilistic convex model process: a new method of time-variant uncertainty analysis and its application to structural dynamic reliability problems, Computer Methods in Applied Mechanics and Engineering 268 (2014) 656–676. doi:https://doi.org/10.1016/j.cma.2013.10.016.

[23] B. Ni, C. Jiang, Interval field model and interval finite element analysis, Computer Methods in Applied Mechanics and Engineering 360 (2020) 112713. doi:https://doi.org/10.1016/j.cma.2019.112713.

[24] M. Faes, M. Imholz, D. Vandepitte, D. Moens, A review of interval field approaches for uncertainty quantification in numerical models, Modern Trends in Structural and Solid Mechanics 3: Non-deterministic Mechanics (2021) 95–110doi:https://doi.org/10.1002/9781119831839.ch6.

[25] A. Sofi, Euler-Bernoulli interval finite element with spatially varying uncertain properties, Acta Mechanica 228 (11) (2017) 3771–3787. doi:https://doi.org/10.1007/s00707-017-1903-7.

[26] C. Jiang, B. Ni, N. Liu, X. Han, J. Liu, Interval process model and non-random vibration analysis, Journal of Sound and Vibration 373 (2016) 104–131. doi:https://doi.org/10.1016/j.jsv.2016.03.019.

[27] Z.-Y. Chen, M. Imholz, L. Li, M. Faes, D. Moens, Transient landing dynamics analysis for a lunar lander with random and interval fields, Applied Mathematical Modelling 88 (2020) 827–851. doi:https://doi.org/10.1016/j.apm.2020.06.075.

[28] L. Piegl, W. Tiller, The NURBS book, Springer Science & Business Media, 1996. doi:https://doi.org/10.1007/978-3-642-59223-2.

[29] J. Li, Y. Cheng, Linear barycentric rational collocation method for solving heat conduction equation, Numerical Methods for Partial Differential Equations 37 (1) (2021) 533–545. doi:http://dx.doi.org/10.1002/num.22539.

[30] K. Shukla, A. D. Jagtap, G. E. Karniadakis, Parallel physics-informed neural networks via domain decomposition, Journal of Computational Physics 447 (2021) 110683. doi:http://dx.doi.org/10.1016/j.jcp.2021.110683.

[31] R. Mittal, R. Jain, Numerical solutions of nonlinear burgers' equation with modified cubic b-splines collocation method, Applied Mathematics and Computation 218 (15) (2012) 7839–7855. doi:https://doi.org/10.1016/j.amc.2012.01.059.
URL https://www.sciencedirect.com/science/article/pii/S0096300312001051

[32] M. P. Bonkile, A. Awasthi, C. Lakshmi, V. Mukundan, V. Aswin, A systematic literature review of burgers' equation with recent advances, Pramana 90 (6) (2018) 1–21. doi:https://doi.org/10.1007/s12043-018-1559-4.

[33] Y. Kim, Y. Choi, D. Widemann, T. Zohdi, A fast and accurate physics-informed neural network reduced order model with shallow masked autoencoder, Journal of Computational Physics 451 (2022) 110841. doi:http://dx.doi.org/10.1016/j.jcp.2021.110841.

[34] F. Yamazaki, M. Shinozuka, G. Dasgupta, Neumann expansion for stochastic finite element analysis, Journal of engineering mechanics 114 (8) (1988) 1335–1354. doi:http://dx.doi.org/10.1061/(ASCE)0733-9399(1988)114:8(1335).

[35] P. Wu, B. Ni, C. Jiang, An interval finite element method based on the neumann series expansion, Chinese journal of theoretical and applied mechanics 52 (5) (2020) 1431–1442. doi:10.6052/0459-1879-20-152.